

Spectral heterogeneity from the spaceborne imaging spectrometer EnMAP reveals biodiversity patterns in forest ecosystems

Michele Torresani ^{a,b}*, Christian Rossi ^{c,d}, Marco Mina ^e, Irene Menegaldo ^a, Matteo Cappuccio ^a, Michela Perrone ^{f,a}, Christopher R. Hakkenberg ^{g,h}, Duccio Rocchini ^{f,i}, Nicola Puletti ^j, Laura Stendardi ^{k,l}, Leonardo Montagnani ^a, Roberto Tognetti ^{a,b}

^a Free University of Bozen/Bolzano, Faculty of Agricultural, Environmental and Food Sciences, Piazza Università/Universitätsplatz, 39100, Bozen/Bolzano, Italy

^b Competence Centre for Plant Health, Piazza Università 5, 39100 Bolzano, Italy

^c Swiss National Park, Department of Geoinformation, Runatsch 124-Chastè Planta-Wildenberg, 7530 Zernez, Switzerland

^d University of Zurich, Department of Geography, Winterthurerstrasse 190, 8057 Zurich, Switzerland

^e Eurac Research, Institute for Alpine Environment, viale Druso 1, Bolzano/Bolzano, Italy

^f Czech University of Life Sciences Prague, Department of Spatial Sciences, Kamýcká 129, 165 00 Praha-Suchdol, Czech Republic

^g Northern Arizona University, School of Informatics, Computing & Cyber Systems, USA

^h University of California at Los Angeles (UCLA), Department of Geography, 315 Portola Plaza, Los Angeles, CA, USA

ⁱ Alma Mater Studiorum University of Bologna, BIOME Lab, Department of Biological, Geological and Environmental Sciences, Via Irnerio 42, 40126 Bologna, Italy

^j CREA, Research Centre for Forestry and Wood, Viale Santa Margherita 80, IT-52100, Arezzo, Italy

^k Eurac Research, Institute for Earth Observation, Viale Druso, 1, Bozen-Bolzano, 39100, Italy

^l University of Florence, Department of Agriculture, Food, Environment, and Forestry (DAGRI), Florence, Italy

ARTICLE INFO

Keywords:

Forest biodiversity
EnMAP
Hyperspectral data
LiDAR
Remote sensing
Spectral diversity

ABSTRACT

The Spectral Variation Hypothesis (SVH) proposes that spectral heterogeneity (SH), derived from optical data, can serve as a proxy for estimating biodiversity. In this study, we tested the SVH across 42 forest plots in the Italian Alps using imaging spectroscopy data from the EnMAP satellite. We investigated the relationship between SH—quantified using two different metrics, Rao's Q and the coefficient of variation (CV)—and tree species diversity (using Shannon's H index and species richness). We applied three levels of spectral analysis: (1) SH calculated for each individual EnMAP band; (2) SH aggregated across broader spectral ranges (Visible -VIS-, Near Infrared -NIR-, and Shortwave Infrared -SWIR-) and (3) SH derived from vegetation indices (VIs). These analyses were performed under three spatial approaches: (A) a normal approach assigning equal weight to all four EnMAP pixels intersecting a plot; (B) a weighted approach based on the proportional overlap of each pixel with the plot area; and (C) a weighted canopy cover (CC)>70% approach, which included only plots with CC greater than 70% as derived from airborne laser scanning (ALS) LiDAR data.

Weak to moderate correlations were observed when SH was derived from single bands, with the strongest relationships in the NIR (R^2 approaching 0.4), followed by the VIS and SWIR regions. A similar trend emerged when SH was aggregated across broader spectral ranges, with the highest correlations again found in the NIR (R^2 up to 0.35). In contrast, lower R^2 values were obtained when SH was computed from specific VIs.

The weighted approaches, especially when restricted to plots with CC >70%, consistently yielded higher R^2 values than the equal-weight approach in all three the spectral analysis. Results were consistent across both SH metrics (Rao's Q and CV), with stronger correlations when species richness was used as the biodiversity metric. This work highlights how EnMAP hyperspectral data, despite inherent constraints, can provide valuable insights into forest biodiversity monitoring.

* Corresponding author at: Free University of Bozen/Bolzano, Faculty of Agricultural, Environmental and Food Sciences, Piazza Università/Universitätsplatz, 39100, Bozen/Bolzano, Italy.

E-mail address: michele.torresani@unibz.it (M. Torresani).

1. Introduction

Despite decades of research, biodiversity remains one of the most complex and dynamic scientific frontiers, with countless species and interactions still undiscovered (Moura and Jetz, 2021; Cazzolla Gatti et al., 2022). Filling these knowledge gaps is essential for understanding how ecosystem functions can be managed sustainably, particularly as species disappear before their ecological roles are fully identified.

In particular, forest ecosystems are recognized as the most biodiverse terrestrial biome, where biodiversity plays a crucial role. Numerous studies have demonstrated that biodiversity within forests enhances ecosystem multi-functionality, including increased carbon uptake (van der Sande et al., 2017) and improved hydrological regulation (Esquivel et al., 2020). These ecosystem services, alongside others such as nutrient cycling, habitat provision, and climate regulation, highlight the essential value of biodiversity in forest ecosystems (Brokerhoff et al., 2017).

Typically, biodiversity monitoring approaches rely on expert-led field inventories, which, while accurate, are time-consuming, costly, and subject to biases (Rocchini et al., 2022). Variability in biodiversity monitoring strategies across countries further complicates data standardization and sharing (Affinito et al., 2024; Moudry et al., 2024a). Recently, earth observation has emerged as a robust tool for the monitoring of different aspects of biodiversity, offering uniform, periodic, and cost-effective data collection, facilitated by advancements in sensor technology and open-access policies for diverse remote sensing data (Nagendra, 2001; Turner et al., 2003; Cavender-Bares et al., 2022; Gatti et al., 2025; Reddy, 2021). Various remote sensing datasets, including optical data from aerial (Gholizadeh et al., 2019; Schweiger and Laliberté, 2022), UAV (Rossi et al., 2021b; Torresani et al., 2023a), and satellite platforms (Rossi et al., 2021a; Pacheco-Labrador et al., 2022), as well as LiDAR (Moudry et al., 2024b) and radar data (Bae et al., 2019), have demonstrated remarkable potential in estimating biodiversity metrics in diverse ecosystems (Hakkenberg et al., 2018).

Focusing on optical remote sensing data, numerous methodologies have been developed to use diverse optical images for estimating biodiversity metrics across ecosystems. Some methods focus on directly mapping specific targets, such as individual tree species or populations (Onishi and Ise, 2021). Others assess the functional component of biodiversity by estimating plant functional traits (Zhao et al., 2021) or by mapping habitats based on climatic/topographic conditions and derived land cover types (Foody, 2008; Stein et al., 2014). Additionally, some approaches explore relationships between *in-situ* biodiversity and spectral reflectance patterns observed in optical imagery (Turner et al., 2003; White et al., 2010). The Spectral Variation Hypothesis (SVH) represents this latter group. SVH utilizes spectral heterogeneity (SH), namely the variability of pixel values, to test, analyze and predict biodiversity patterns (Torresani et al., 2024c). This approach states that the diversity in spectral responses detected by optical sensors can serve as a proxy for estimating biodiversity, including alpha diversity (within-site diversity), beta diversity (variation between sites), and gamma diversity (total landscape diversity). Specifically focusing on alpha diversity, the hypothesis suggests that areas with high SH in remotely sensed imagery correspond to greater environmental heterogeneity (and ecological niche diversity), which supports higher species richness compared to areas with low SH (Palmer et al., 2002; Rocchini et al., 2010; Torresani et al., 2024c).

The SVH has been extensively tested across diverse ecosystems, employing various types of optical data, testing different SH metrics (e.g. coefficient of variation CV Gholizadeh et al., 2019, the Rao's Q index Thouverai et al., 2021, the mean distance from centroids Rocchini et al., 2004), and methodological approaches. As highlighted in the recent review of the SVH by Torresani et al. (2024c), most studies testing the SVH have reported significant results, supporting its validity across diverse ecosystems. However, some studies have reported nonsignificant results (Schmidlein and Fasnacht, 2017; Jung, 2022;

Lopes et al., 2017), highlighting that the applicability and reliability of the SVH can be significantly influenced by various factors. These include the selection of SH metrics, the ecosystem being assessed, and the habitat type (Fasnacht et al., 2022). Additional factors such as the design of moving windows (Conti et al., 2021), field data collection methodologies—including the choice of diversity indices (e.g., species richness or Shannon's H index) and sampling design—vegetation phenology (Perrone et al., 2024), and structural complexity (e.g., biomass Rossi et al., 2021b, density Van Cleemput et al., 2023, diversity in plant height Conti et al., 2021 and soil characteristics Gholizadeh et al., 2018a) further complicate the application of the SVH. These elements influence both spectral reflectance and biodiversity patterns, making it crucial to account for these variables in future studies. Lastly, and maybe the most important factor is the characteristics of optical images, such as spectral (Wang et al., 2018b, 2022a), spatial (Torresani et al., 2018; Rossi et al., 2021b), and temporal resolution (Torresani et al., 2019; Wang et al., 2022b; Rossi et al., 2024).

On this topic, studies have explored hypothesis using data from different platforms, including UAVs (Rossi et al., 2021b), airborne systems (Wang et al., 2016), and satellites (Perrone et al., 2023), using multispectral and hyperspectral data. These studies demonstrate the versatility of the SVH but also reveal variability in its effectiveness depending on the platform, data characteristics, and methodological approach (Torresani et al., 2024c). Focusing on optical spaceborne data, several studies have tested the SVH using satellite imagery. Initially, the SVH was tested with Landsat data. After 2015, Sentinel-2 has become the most widely-used satellite for biodiversity estimation through the SVH, owing to its high spatial, spectral, and temporal resolution. Other satellites, such as MODIS (Rocchini et al., 2014), WorldView (Mapfumo et al., 2016), QuickBird (Hall et al., 2010) and others, have also been employed to test the SVH, though their application has been less extensive (Torresani et al., 2024c).

Recently, a new hyperspectral satellite, the Environmental Mapping and Analysis Program (EnMAP), has been launched to advance the monitoring and analysis of Earth's surface (Kaufmann et al., 2006). Launched in 2022 to provide advanced imaging capabilities, EnMAP captures data across a wide spectral range, covering the Visible (VIS), Near Infrared (NIR), Short Wave Infrared (SWIR) regions (from 420 nm to 2450 nm) with 242 contiguous spectral bands. Each band has a spectral sampling interval of approximately 6.5 nm in the VIS and NIR and approximately 10 nm in the SWIR, enabling detailed analysis of surface characteristics. EnMAP's spatial resolution is 30 m, and it features a swath width of 30 km, making it suitable for large-scale environmental and ecological studies (ESA eoPortal, 2025).

Several studies have explored the SVH using spaceborne imaging spectroscopy data, particularly from satellites such as DESIS (Rossi and Gholizadeh, 2023; Gholizadeh et al., 2022) and Zhuhai-1 (Wang et al., 2022a). These studies have demonstrated the potential of imaging spectroscopy for assessing SH and its relationship with ecological patterns. However, to date, no studies have specifically tested the SVH using EnMAP data for biodiversity estimation, particularly in the context of tree species diversity estimation within forest ecosystems. This gap presents a valuable opportunity to explore the application of spaceborne hyperspectral data for detecting species diversity and ecological processes in these highly diverse environments.

Another critical factor influencing the relationship between SH and species diversity is the interplay between vegetation structure (e.g., canopy cover and complexity) of the ecosystem being analyzed versus the spatial resolution of the optical data used. When using data with a spatial resolution of 30 m, such as EnMAP, there is a risk of analyzing forested areas that may also include non-forested patches, potentially introducing bias into the results. This issue is particularly relevant in heterogeneous landscapes where mixed land cover types are more likely to occur within a single pixel. This aspect remains a topic of active debate within the context of the SVH, with some recent studies already investigating its implications and potential solutions

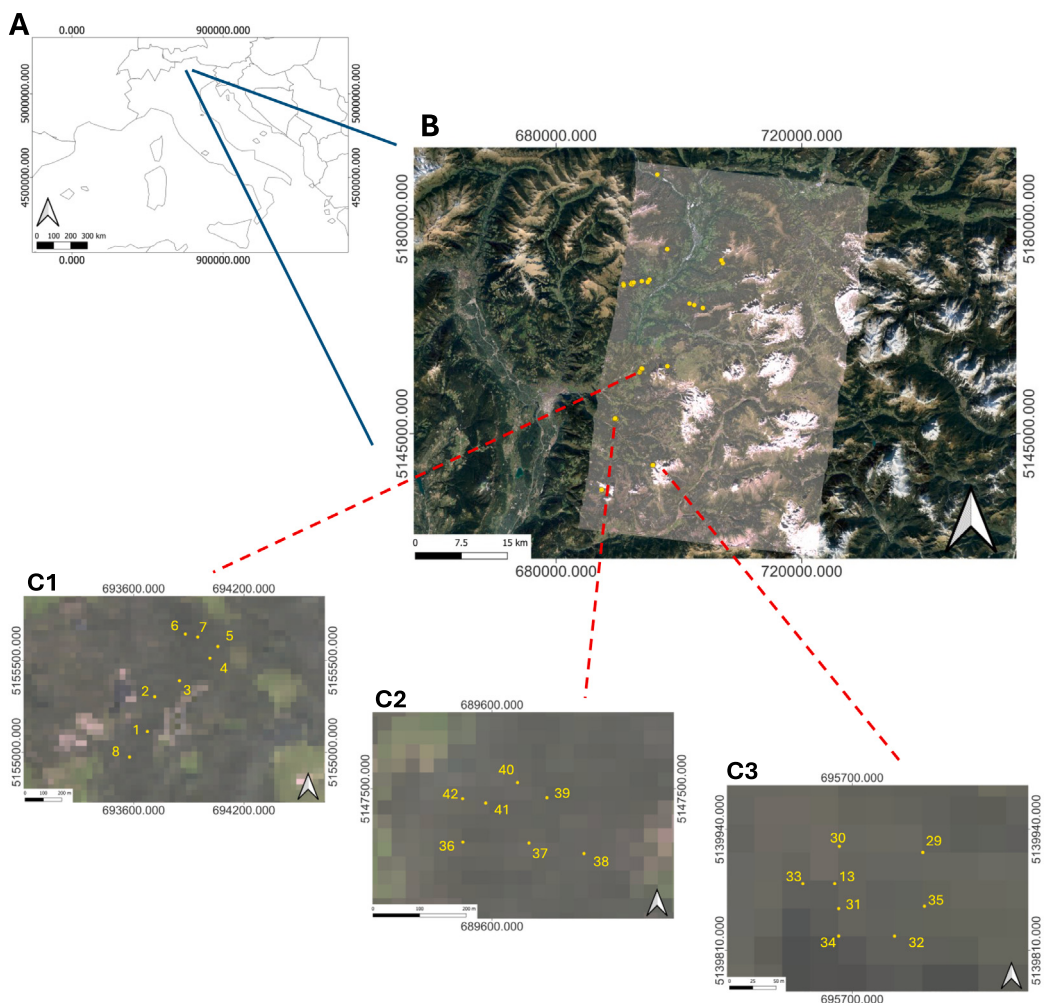


Fig. 1. (A) Location of the plots within the Italian borders. (B) Location of the entire study area with forest sampling plots, with the RGB EnMAP tiles used for the analysis shown over a Google Earth image. (C1–C3) Zooms on three sub-areas where the location of individual sampling plots could not be distinguished in panel (B). Plot IDs (numeric labels) are indicated in yellow. (For interpretation of the references to color in this figure legend, the reader is referred to the web version of this article.)

(Gholizadeh et al., 2018b; Hauser et al., 2021; Van Cleemput et al., 2023).

The aim of this study is to investigate whether SH from the new German spaceborne hyperspectral mission EnMAP can be applied to map tree species diversity in mountain forests of the Italian Alps. Specifically, we examine whether SH, calculated using two widely applied indices, Rao's Q and the CV, is correlated with tree species diversity, assessed using two complementary field-based metrics: species richness and Shannon's H index. To comprehensively test the SVH, we applied three levels of spectral analysis: (1) SH calculated at the individual band level for each of the EnMAP bands; (2) SH aggregated across broader spectral ranges—namely the VIS, NIR, and SWIR regions; and (3) SH derived from a set of vegetation indices (VIs) that capture ecologically relevant traits such as chlorophyll content, water status, and canopy structure. Furthermore, to evaluate how spatial detail and tree density influence SH-diversity relationships, we tested the above mentioned analysis with three different spatial approaches: (A) a normal (equal-weight) approach, where each of the four EnMAP pixels overlapping a plot was considered equally; (B) a weighted-area approach, in which pixels were weighted according to their proportional overlap with the plot area; and (C) a weighted-area approach restricted to high canopy cover (CC), where only plots with CC greater than 70%—as derived from airborne laser scanning (ALS) LiDAR data—were included in the analysis. By exploring these combinations, we aim to

identify the most effective approach for linking spaceborne imaging spectroscopy SH to tree species diversity in forested landscapes.

2. Material and methods

2.1. Study area and field data collection

The study area is located in a portion of South Tyrol, a region in northern Italy corresponding to the Autonomous Province of Bolzano/Bozen. A total of 52 forest sampling plots were used for the analysis. The geographic coordinates of the plots were collected using an RTK GPS with a positional accuracy of <20 cm, ensuring high-precision matching with the EnMAP data. The plots are originated from different projects that shared a common study design; therefore, no unified sampling layout was applied across the entire dataset. In each plot with a radius of 13 m, between 2021 and 2024 all trees with a diameter at breast height (DBH) greater than 10 cm were identified and categorized by species. Following a preprocessing phase—described in detail in subsequent sections, 10 plots were excluded from the analysis due to the presence of corrupted or missing spectral bands in the corresponding EnMAP data. Consequently, the final analysis was conducted on 42 plots for which both high-quality spectral and field data were available (Fig. 1). To evaluate potential spatial autocorrelation among plots, we performed a Moran's I analysis, which indicated no significant

spatial autocorrelation. The full results of this test are reported in the Appendix.

2.2. In-situ tree species diversity estimation

Using the measurements of individual trees in each sampling plot, we calculated two indices of tree species diversity: species richness and Shannon's H.

Species richness was derived by summing the number of tree species per each plot, while Shannon's H (Eq. (1)) is a widely used metric in ecology for assessing alpha diversity that originally emanates from information theory. This index incorporates both the abundance of each species and the evenness of their distribution within an area, providing a more nuanced measure of diversity (Shannon, 1948).

$$H = - \sum_{i=1}^q p_i * \ln(p_i) \quad (1)$$

where:

- H = Shannon's diversity index
- q = number of observed species
- p_i = proportion of individuals belonging to species i relative to the total number of individuals in the plot.

2.3. EnMAP data and pre-processing analysis

For this study, we utilized a single EnMAP acquisition collected on September 9, 2023. The dataset consisted of two adjacent tiles (DT0000041009_20230909T102950Z_001 and DT0000041009_20230909T102950Z_002), both processed to Level 2A (Chabrilat et al., 2024) on September 10, 2023. The images were downloaded from the EnMAP Instrument Planning portal (<https://planning.enmap.org/>). The level 2A products are atmospherically corrected using the official EnMAP Ground Segment processing chain, as described in the EnMAP L2A Processor ATBD (EnMAP Ground Segment Team, 2023). This correction includes radiative transfer-based inversion algorithms that retrieve surface reflectance values over land by accounting for atmospheric effects such as aerosol scattering and water vapor absorption. Specifically, aerosol optical thickness at 550 nm is retrieved using a dense dark vegetation approach, while columnar water vapor is estimated per pixel with the Atmospheric Pre-corrected Differential Absorption method. The resulting surface reflectance values are expressed in percent units. Spectral smile correction and interpolation of defective pixels were also applied during Level 1B intermediate processing to improve the spectral integrity and continuity of the reflectance data.

For each plot, we extracted the reflectance values of the four EnMAP pixels surrounding the plot center. The mean reflectance was calculated across these four pixels for each spectral band, generating a single representative spectral signature per plot. Subsequently, following the study of Rossi and Gholizadeh (2023) noisy bands due to sensor performance or suboptimal atmospheric correction were identified and removed before further analysis. Specifically, we discarded bands 1–2 (from 418 nm to 420 nm), bands 79–103 (from 895 nm to 1014 nm), bands 131–135 (missing values, from 1342 nm to 1390 nm), bands 167–175 (from 1967 nm to 2041 nm), and bands 222–225 (from 2430 nm to 2445 nm). After this preprocessing step, a total of 219 spectral bands were retained for subsequent analysis. The spectral regions excluded and the overall spectral signature after preprocessing are illustrated in Fig. 2.

2.4. Spectral heterogeneity indices

The SH was calculated using two established metrics: Rao's Q index and the CV. The Rao's Q index (Eq. (2)) was originally developed by Rao (1982) and later proposed by Botta-Dukát (2005) as a functional diversity index in ecology. Rocchini et al. (2024) adapted this metric for remote sensing applications as a measure of SH, calculated using the following formula:

$$Q = \sum_{i,j=1}^N d_{ij} \times p_i \times p_j \quad (2)$$

where:

- Q : Rao's Q index, used in remote sensing applications.
- p_i and p_j : Relative abundance of pixels i and j in a selected area (e.g., region of interest or raster) with N total pixels ($p_i = p_j = 1/N$).
- d_{ij} : Distance or dissimilarity between pixels i and j , where $d_{ij} = d_{ji}$ and $d_{ii} = 0$.

In this study, d_{ij} was calculated, as done in other studies (Torresani et al., 2024a; Pafumi et al., 2023) as the Euclidean distance based on a single spectral layer.

The CV (Eq. (3)) is another commonly used heterogeneity index in ecological remote sensing research (Rossi and Gholizadeh, 2023; Rahamanian et al., 2023). It was calculated as follows:

$$CV = SD/\bar{x} \quad (3)$$

where:

- CV : Coefficient of Variation of spectral reflectance.
- SD : Standard deviation of spectral reflectance values within the selected area.
- \bar{x} : Mean spectral reflectance value within the selected area.

2.5. Spectral heterogeneity analysis

To assess the relationship between SH and tree species diversity, SH was computed with the above-mentioned SH indices (Rao's Q and CV) using three different spectral analyses:

2.5.1. SH at the individual band level

The first analysis aimed to test the SVH using each EnMAP band. For all bands (excluding those identified as unsuitable during the band selection process), we calculated SH using the Rao's Q and the CV. The resulting SH values were then correlated by linear regression with tree species diversity, measured using Shannon's H index and species richness. For each regression, the coefficient of determination (R^2) and slope were computed to evaluate the strength and direction of the relationship between SH and tree species diversity.

2.5.2. SH across spectral ranges

Following the work of Wang et al. (2016, 2018a) we aimed to analyze the SVH by assessing the SH across the following spectral ranges (rather than individual bands):

- VIS: Covering bands from 400–700 nm.
- NIR: Covering bands from 700–900 nm.
- SWIR: Covering bands from 1000–2500 nm.

SH was computed with a modified CV formula (formula 2.5.2) and a modified Rao's Q formula (formula 2.5.2) indices within each spectral region for each plot as follows:

$$CV_{\text{mean}} = \frac{\sum_{\lambda=1}^n \frac{sd(\rho_\lambda)}{\text{mean}(\rho_\lambda)}}{n}$$

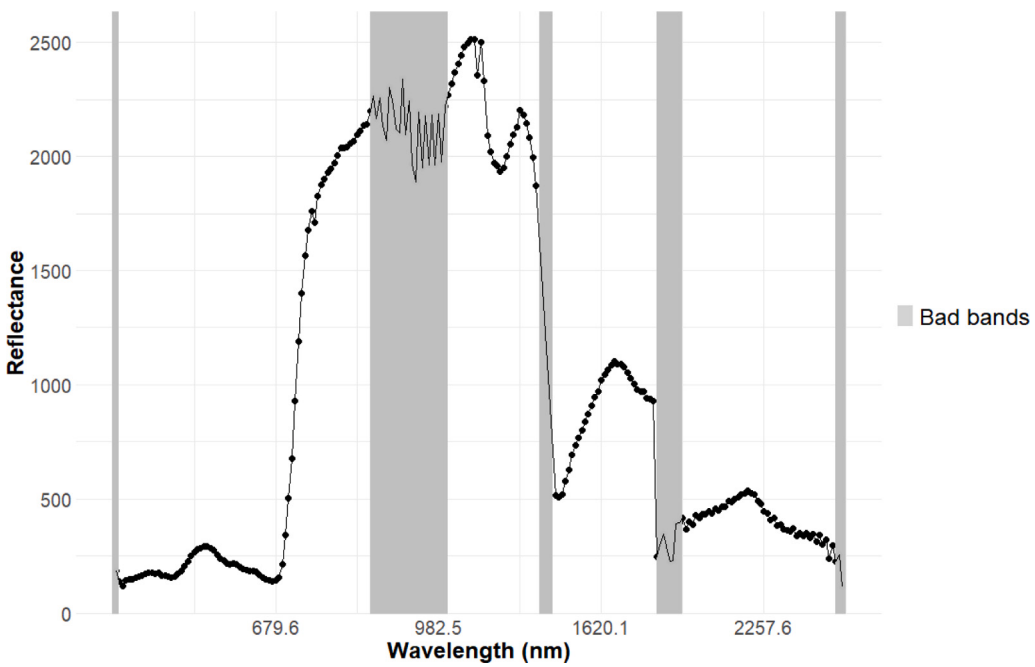


Fig. 2. Mean spectral signature calculated from the average reflectance values of the EnMAP pixels. The shaded gray regions represent the ‘bad bands’ 1–2 (from 418 nm to 420 nm), bands 79–103 (from 895 nm to 1014 nm), bands 131–135 (missing values, from 1342 nm to 1390 nm), bands 167–175 (from 1967 nm to 2041 nm), and bands 222–225 (from 2430 nm to 2445 nm) that were excluded from our analysis.

where $\text{sd}(\rho_\lambda)$ is the standard deviation of reflectance values across the four pixels in each plot for the λ th spectral band, $\text{mean}(\rho_\lambda)$ is the mean reflectance for the same band and pixels, and n is the total number of bands in the respective spectral range (Levin et al., 2007; Gholizadeh et al., 2018a).

$$Q_{\text{mean}} = \frac{\sum_{\lambda=1}^n \frac{\sum_{i=1}^N \sum_{j=1}^N d_{ij}^\lambda}{N^2}}{n}$$

where:

- Q_{mean} : The average Rao’s Q index for a plot across all spectral bands.
- n : The total number of spectral bands in the respective spectral range.
- N : The total number of pixels in the plot.
- d_{ij}^λ : The pairwise Euclidean distance between reflectance values of pixels i and j for the λ th spectral band.

As for the single band analysis, the resulting SH values were correlated with tree species diversity, measured using Shannon’s H index and species richness, through linear regression deriving R^2 (coefficient of determination) and slope.

2.5.3. SH of EnMAP derived vegetation indices

Lastly, we analyzed the SVH by assessing the SH using 10 VIs, derived from the following EnMAP bands (see Table 1):

The choice of bands was made by selecting the EnMAP band whose central wavelength most closely matched the reference wavelength specified in the original index formulation. See Appendix 1 for the list of the vegetation index formulas with corresponding EnMAP band numbers, and literature references.

For each VI, SH was calculated using both Rao’s Q and CV indices, and its correlation with tree species diversity indices (Shannon’s H and species richness) was tested, as previously done, through linear regression deriving R^2 and slope. For CV, the absolute mean was used to ensure stable estimates even when VI values were negative.

2.6. Analytical approaches

Each forest plot had a 26-m diameter, while the EnMAP pixel size was 30×30 m, meaning that the SH calculations were based on the four EnMAP pixels intersecting the plot. To account for the misalignment between plot size and pixel resolution, we implemented and compared three different approaches (Fig. 3):

- **Normal - Equal weight approach** – Each of the four EnMAP pixels intersecting the plot was given an equal weight when computing SH.
- **Weighted-area approach** – Instead of assigning equal weights, we calculated the proportional area of the plot covered by each pixel and applied these weights when computing SH. This approach ensures that pixels contributing more to the plot area influence SH calculations proportionally, reducing bias from pixels that are only partially intersected by the plot boundary.

The weighted-area approach was implemented by extracting reflectance values from the four EnMAP pixels, calculating the proportion of each pixel that overlapped with the field plot, and applying these proportions when computing SH using both Rao’s Q and CV. This method improves the precision of SH estimates by aligning them more closely with the actual area surveyed in the field.

For the weighted CV, following the work of Wang et al. (2016, 2018a) we modified the standard CV formula to account for the area proportion (w_i) of each pixel within the plot:

$$CV_{\text{weighted}} = \frac{\sqrt{\sum_{i=1}^N w_i (\rho_i - \mu_w)^2 / \sum_{i=1}^N w_i}}{\mu_w} \times 100 \quad (4)$$

where the weighted mean reflectance (μ_w) is calculated as:

$$\mu_w = \frac{\sum_{i=1}^N w_i \cdot \rho_i}{\sum_{i=1}^N w_i} \quad (5)$$

Table 1

Vegetation indices used in the study, their primary ecological linkages, key traits, and corresponding formulas based on EnMAP wavelengths (nm). For completeness, the same information is also provided in the Appendix with the corresponding EnMAP band numbers and references.

Index	Primary ecological link	Key traits/Properties	Formula
NDVI	Vegetation health	Chlorophyll, photosynthetic activity, biomass	$\frac{801.25 \text{ nm} - 673.13 \text{ nm}}{801.25 \text{ nm} + 673.13 \text{ nm}}$
EVI	Productivity, canopy structure	Chlorophyll, photosynthetic efficiency	$2.5 \times \frac{801.25 \text{ nm} - 673.13 \text{ nm}}{801.25 \text{ nm} + 6 \times 673.13 \text{ nm} - 7.5 \times 454.31 \text{ nm} + 1}$
TGI	Leaf chlorophyll	Chlorophyll concentration	$-0.5 \times [190(673.13 \text{ nm} - 550.69 \text{ nm}) - 120(673.13 \text{ nm} - 482.41 \text{ nm})]$
TCARI	Chlorophyll absorption, stress	Chlorophyll, nitrogen, photosynthetic capacity	$3 \times \frac{(699.78 \text{ nm} - 673.13 \text{ nm}) - 0.2(699.78 \text{ nm} - 550.69 \text{ nm})}{699.78 \text{ nm}/673.13 \text{ nm}}$
NDWI	Water content	Vegetation hydration, drought stress	$\frac{879.69 \text{ nm} - 1270.92 \text{ nm}}{879.69 \text{ nm} + 1270.92 \text{ nm}}$
DSWI	Water content	Dryness stress	$\frac{801.25 \text{ nm} + 545.55 \text{ nm}}{1211.05 \text{ nm} + 679.69 \text{ nm}}$
SIPI1	Carotenoid content, stress	Carotenoids, photosynthetic efficiency	$\frac{801.25 \text{ nm} - 444.70 \text{ nm}}{801.25 \text{ nm} - 679.69 \text{ nm}}$
CRI1	Carotenoid content, stress	Carotenoids, stress response, senescence	$\frac{1}{510.83 \text{ nm}} - \frac{1}{550.69 \text{ nm}}$
SIPI2	Carotenoid content, stress	Anthocyanin accumulation	$\frac{801.25 \text{ nm} - 506.02 \text{ nm}}{801.25 \text{ nm} - 693.01 \text{ nm}}$
BGI	Dry matter	Lignin and cellulose content	$\frac{449.54 \text{ nm}}{550.69 \text{ nm}}$
CUR	Fluorescence	Photochemical reflectance	$673.13 \text{ nm} \times \frac{693.01 \text{ nm}}{(686.32 \text{ nm})^2}$

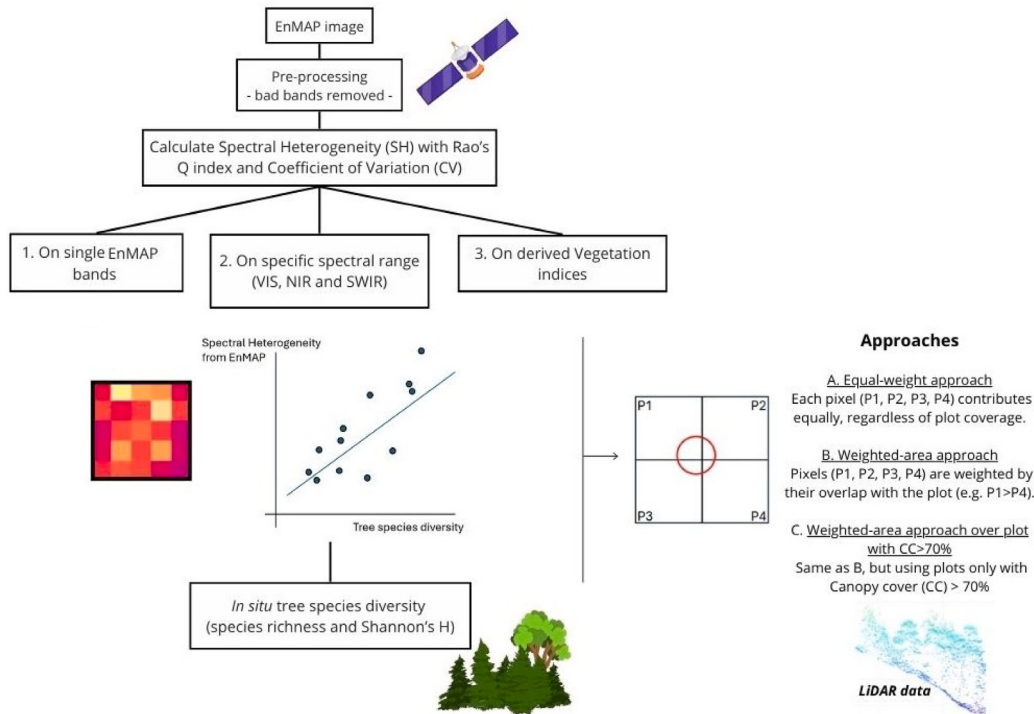


Fig. 3. Workflow for testing the spectral variation hypothesis using EnMAP data. Spectral heterogeneity is calculated from pre-processed EnMAP imagery using Rao's Q and the Coefficient of Variation on (1) single bands, (2) specific spectral ranges (VIS, NIR, SWIR), and (3) vegetation indices. The resulting spectral heterogeneity values are correlated with in situ tree species diversity (species richness and Shannon's H). To account for the misalignment between plot size (26 m diameter) and pixel resolution (30 m) three approaches are used: (A) an equal-weight approach where all four pixels (P1, P2, P3, P4) contribute equally, and (B) a weighted-area approach where pixels are weighted based on their overlap with the plot (e.g., P1 > P4) and (C) a refined weighted-area approach that includes only plots with a canopy cover greater than 70% estimated using LiDAR ALS data.

where:

- ρ_i is the reflectance value of pixel i .
- w_i is the proportional area of the plot covered by pixel i .
- μ_w is the weighted mean reflectance across the plot.

For the weighted Rao's Q, we adapted the classical formulation of Rao's quadratic entropy, where abundances (p_i) are defined

as the relative contribution of each pixel to the plot area ($p_i = w_i / \sum w_k$). This ensures that each pixel contributes proportionally to its overlap with the plot. The resulting weighted Rao's Q for band λ is given by:

$$Q_{\text{weighted}}^{\lambda} = \frac{\sum_{i=1}^N \sum_{j=1}^N w_i w_j d_{ij}^{\lambda}}{\left(\sum_{k=1}^N w_k\right)^2}, \quad (6)$$

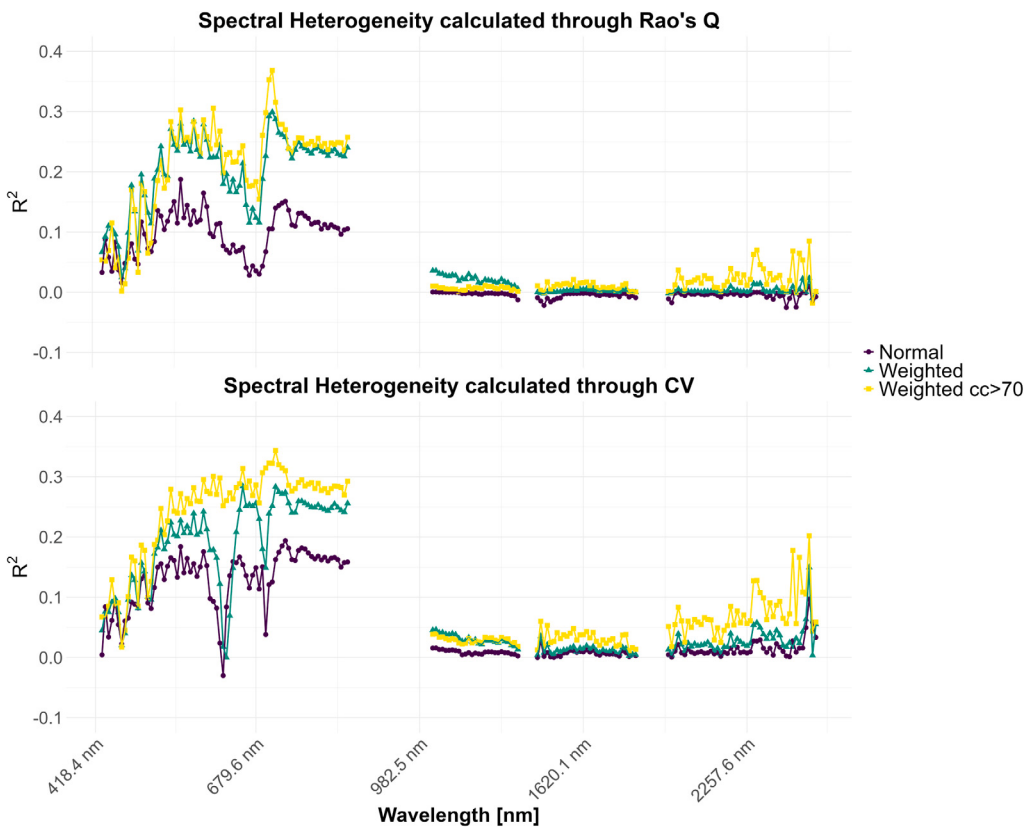


Fig. 4. R^2 (coefficient of determination) values from the correlation between spectral heterogeneity (Rao's Q and CV), calculated for individual EnMAP bands, and tree species diversity measured using the species richness. The three approaches compared include: 'normal' (unweighted, in dark blue), 'weighted' (accounting for pixel overlap, in green), and 'weighted CC > 70%' (restricted to plots with canopy cover > 70%, in yellow). The top panel presents results using Rao's Q, while the bottom panel shows results using the coefficient of variation (CV). Negative R^2 values indicate negative correlations.

where w_i and w_j are the proportional overlaps of pixels i and j with the plot, and d_{ij}^λ is the pairwise Euclidean distance between reflectance values of pixels i and j for band λ . To obtain spectral-range level estimates (e.g., VIS, NIR, SWIR), we averaged $Q_{\text{weighted}}^\lambda$ across all bands in the respective range:

$$Q_{\text{weighted}} = \frac{1}{n} \sum_{\lambda=1}^n Q_{\text{weighted}}^\lambda. \quad (7)$$

- **Weighted-area approach considering plots with CC > 70%** – This approach builds on the weighted-area method but includes only those plots with a CC greater than 70%. The goal is to evaluate the influence of tree density and structural complexity on the relationship between SH and biodiversity by focusing on denser plots.

2.7. LiDAR data and canopy cover estimation

In order to calculate the CC, we used local ALS LiDAR data. The data were acquired during an ALS campaign conducted in 2006 by the Province of Bolzano/Bozen (freely available here: <http://geocatalogo.retecivica.bz.it/geokatalog/>). The Canopy height Models (CHMs) were derived from the ALS point cloud data using the R package "lidR". First, ground points were classified using the `classify_ground()` function with the `pmf()` algorithm. The height normalization was then performed with the `normalize_height()` function, employing the `knnidw()` algorithm. Noise and points with heights below 0 m or above 50 m were filtered out using `filter_poi()`. Successively, the CHMs were generated with a spatial resolution of 2.5 m (the highest resolution possible due to the number of points per square

meter) using the `rasterize_canopy()` function with the `p2r()` algorithm. Following the methodology of previous works (Torresani et al., 2020, 2023b), the CC for each plot was calculated using the following formula:

$$CC = \frac{px_{2m}}{px_{tot}} \times 100$$

where:

- CC: Canopy cover, expressed as a percentage.
- px_{2m} : Number of pixels in a CHM with a value greater than 2 m.
- px_{tot} : Total number of pixels in the plot.

3. Results

3.1. Forest plot diversity and structural attributes

The forest plots included in this study represent a broad gradient of tree species diversity and structural complexity. Tree species richness, recorded within each 26-m diameter plot, ranged from 1 to 4 species. This relatively low but variable richness reflects the typical composition of temperate and subalpine forest communities in the Italian Alps. In terms of species evenness, measured by the Shannon's H , values ranged from a minimum of 0.14 to a maximum of 1.36, indicating a spectrum from monospecific or uneven communities to more diverse and balanced assemblages. CC derived from ALS LiDAR data, also showed substantial variability, ranging from 41.4% to 96.5%. This variation highlights differences in tree density and structure among plots, which are expected to influence the spectral signal captured by the EnMAP satellite and, consequently, the SH. Full information about each plot (location, species richness, Shannon's H and CC) is provided in the Appendix (Table A1).

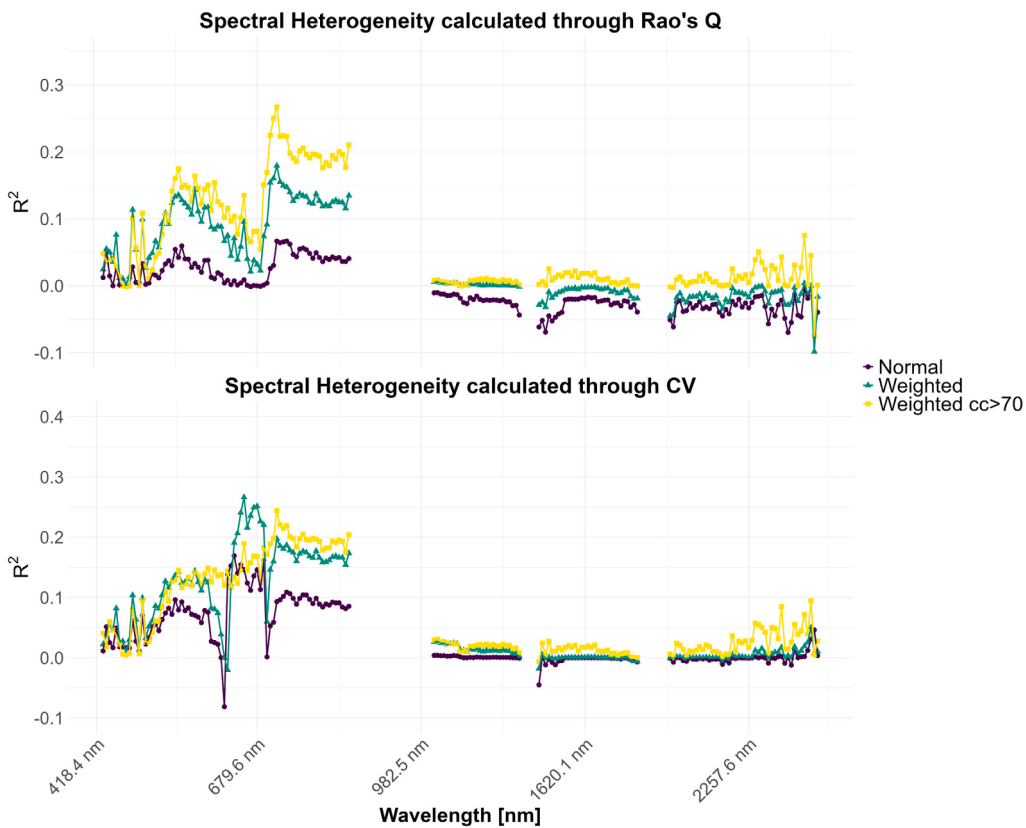


Fig. 5. R^2 (coefficient of determination) values from the correlation between spectral heterogeneity (Rao's Q and CV), calculated for individual EnMAP bands, and tree species diversity measured using Shannon's H index. The three approaches compared include: 'normal' (unweighted, in dark blue), 'weighted' (accounting for pixel overlap, in green), and 'weighted CC > 70%' (restricted to plots with canopy cover > 70%, in yellow). The top panel presents results using Rao's Q, while the bottom panel shows results using the coefficient of variation (CV). Negative R^2 values indicate negative correlations.

3.2. Single bands analysis

The coefficient of determination (R^2 values, y-axis) between tree species diversity, measured using species richness, and SH measured using the Rao's Q index (above) and the CV (below), calculated for each individual EnMAP band (x-axis) are presented in Fig. 4. The three different approaches (normal approach, weighted approach and the weighted approach limited to plots with CC greater than 70%) were compared. R^2 values vary across the spectral bands for all three approaches considered and they were generally very low in the SWIR region—sometimes even negative—slightly higher in the VIS range, and tend to increase in the NIR region. The highest R^2 values, reaching up to 0.38, were obtained using the weighted approach restricted to plots with CC greater than 70%, followed by the standard weighted approach, and lastly the unweighted (normal) method. This pattern is consistent regardless of whether SH is calculated using Rao's Q or the CV.

Similarly, Fig. 5 presents the same analysis, but with tree species diversity measured using Shannon's H index. The results follow a pattern comparable to that observed for species richness, with higher R^2 values in the NIR region and lower values in the SWIR and VIS regions. Overall, the highest correlations are obtained using the weighted approach limited to plots with CC greater than 70%, while the lowest values are observed with the normal approach. Compared to the previous results where species diversity was assessed through species richness, the correlations observed here are generally slightly weaker.

3.3. Spectral range analysis

Correlation analysis (R^2 values with p-values) between tree species diversity—assessed using both Shannon's H index and species

richness—and SH, calculated over three spectral ranges (VIS, NIR, and SWIR) using the three different approaches are shown in Fig. 6.

The results highlight a clear variability in the strength of the correlations depending on both the spectral range and the methodological approach. In general, SH computed in the NIR range shows the highest correlation with tree diversity, followed by VIS and SWIR, which exhibit much weaker or even negative correlations. The best performing approach is the weighted method limited to plots with CC > 70% (highest $R^2 = 0.34$ when SH is assessed with CV in the NIR using the weighted CC > 70% approach), followed by the standard weighted method, while the normal approach consistently shows the weakest correlations. Additionally, species richness tends to yield stronger correlations than Shannon's H, particularly in the NIR range. Similar patterns were obtained regardless of whether SH was calculated using Rao's Q or CV, indicating consistency between the two heterogeneity metrics.

3.4. Vegetation indices analysis

Finally the correlation between tree species diversity, measured using both Shannon's H and species richness, and SH calculated using Rao's Q across various VIs is shown in Fig. 7. Due to space constraints and the similarity of the results, the corresponding CV-based analysis is presented in the Appendix. Consistent with previous analyses, the highest R^2 values are generally obtained using the weighted CC > 70% approach, followed by the weighted and then the normal approach. The goodness of fit are generally low with $R^2 > 0.2$ observed for specific indices, particularly the Triangular Greenness Index (TGI), as well as the Structure Insensitive Pigment Indices (SIP12). As observed in previous analyses, and with the exception of a few indices such as BGI, the correlations are generally stronger when species richness is used as the diversity metric compared to Shannon's H.

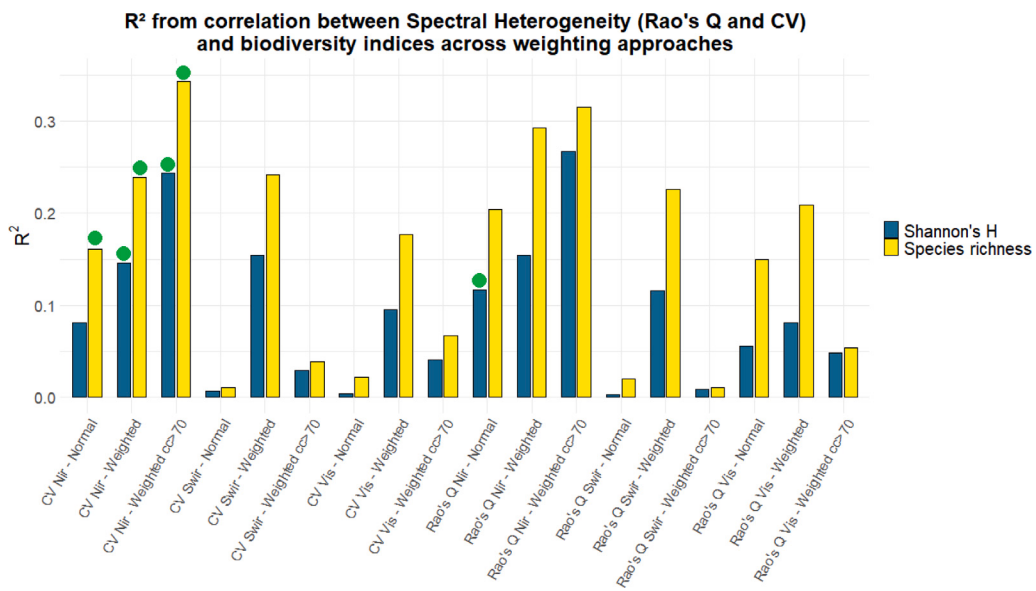


Fig. 6. R^2 (coefficient of determination) values from the correlation between spectral heterogeneity, calculated using Rao's Q and the coefficient of variation (CV), and tree species diversity, measured through Shannon's H index (blue bars) and species richness (yellow bars). SH was computed across three spectral ranges (VIS, NIR, and SWIR) using three different approaches: a normal approach, a weighted approach, and a weighted approach restricted to plots with canopy cover (CC) > 70%. Green dots indicate statistically significant relationships (p -value < 0.05). (For interpretation of the references to color in this figure legend, the reader is referred to the web version of this article.)

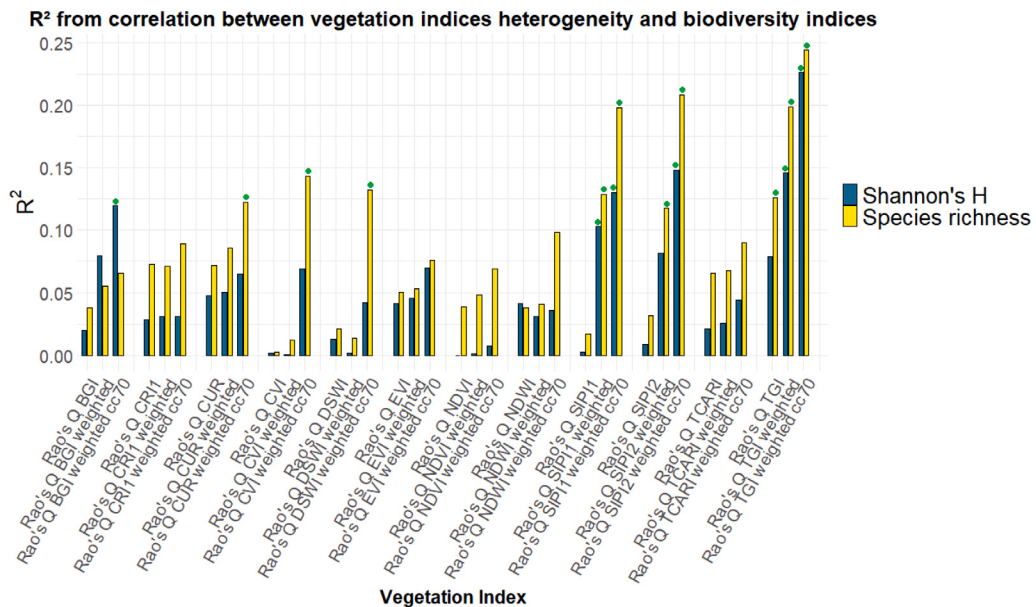


Fig. 7. R^2 (coefficient of determination) values from the correlation between spectral heterogeneity (Rao's Q) of different vegetation indices and tree species diversity metrics (Shannon's H and species richness). Bars indicate the strength of the relationship, with three approaches considered: normal (equal contribution from all EnMAP pixels), weighted (pixels weighted by their overlap with the plot), and weighted CC > 70% (weighted approach limited to plots with canopy cover > 70%). Blue bars represent correlations with Shannon's H, while yellow bars represent correlations with species richness. Green dots indicate statistically significant relationships (p -value < 0.05). (For interpretation of the references to color in this figure legend, the reader is referred to the web version of this article.)

4. Discussion

In this study, we tested the SVH to estimate tree species diversity across various forest plots in the Italian Alps. SH was assessed using hyperspectral data from the new German EnMAP satellite and calculated through two different heterogeneity metrics: Rao's Q index and CV. These SH metrics were then correlated with field-based tree species diversity, measured using two complementary indices—Shannon's H

and species richness. To comprehensively assess the SVH, we applied three levels of spectral analysis: (1) SH calculated at the individual band level for each EnMAP spectral band; (2) SH computed across broader spectral ranges (VIS, NIR, and SWIR); and (3) SH derived from selected VIs related to key ecological traits. We tested these analysis using three spatial approaches to understand the influence of spatial detail and tree density: (A) a normal approach, where each of the four EnMAP pixels overlapping a plot contributed equally; (B) a weighted

approach, where pixels were weighted by their area of overlap with the plot; and (C) a weighted CC > 70% approach, where only plots with CC exceeding 70% (based on ALS data) were included.

4.1. Comparative insights from band-level, spectral range, and VI analyses

Our findings demonstrate that, under certain conditions, SH derived from EnMAP hyperspectral data can effectively predict tree species diversity. Among the three types of analyses conducted, the band-level approach—tested here for the first time using EnMAP spaceborne hyperspectral data, revealed weak to moderate correlations. Specifically, correlations were generally low in the SWIR region, slightly higher in the VIS, and consistently the highest in the NIR bands, across both diversity metrics (species richness and Shannon's H). This is likely due to the fact that NIR reflectance is strongly influenced by internal leaf structure and canopy characteristics, which tend to vary more among different tree species than in other spectral regions (Slaton et al., 2001; Knyazikhin et al., 2013). Such variability in NIR signals may capture subtle differences in species composition, crown architecture, and foliage density—ecological traits closely linked to species diversity.

The analysis based on VIs showed also weak results. Among the tested indices, TGI, Sipi1, and Sipi2 yielded the highest correlations with tree species diversity but the general R^2 remain low.

Interestingly, NDVI—despite its widespread use—showed one of the lowest correlations with species diversity in our study. While several studies have reported strong NDVI-biodiversity relationships (Oindo and Skidmore, 2002; Levin et al., 2007; Helfenstein et al., 2022), others, such as Hakkenberg et al. (2018) and Pinon et al. (2024), have documented weak or negative correlations between NDVI and species richness in structurally complex forests. Pinon et al. (2024) found that in ecosystems with dense and vertically stratified canopies, such as the Atlantic Forest, NDVI can saturate due to high LAI leading to uniformly high NDVI values even when species diversity is high. This saturation effect reduces NDVI's sensitivity to additional increases in biomass or canopy complexity, which may produce a negative or weak relationship with diversity. Moreover, Pinon et al. (2024) highlighted that in forests with multiple vegetation layers, reflectance uniformity across dense canopies can mask species-level heterogeneity, further diminishing the correlation between NDVI and biodiversity metrics. Similar dynamics have been observed in other studies attributing weak NDVI–diversity relationships to canopy shading, layering, and successional stages that modify NIR reflectance patterns (Gillespie, 2005; Schneider et al., 2017). In our alpine forests, characterized by complex vertical structure and heterogeneous canopy layers, these mechanisms likely contribute to the observed weak NDVI–diversity correlations. This underscores the context-dependent performance of NDVI as a biodiversity proxy, influenced by forest structure, canopy complexity, and the potential for NDVI saturation in high-biomass systems. The timing of data acquisition in September may have influenced NDVI's limited ability to capture interspecific variability, particularly in conifer-dominated alpine ecosystems. According to previous studies that tested the SVH in the same region (Torresani et al., 2019, 2018), the peak of vegetation activity typically occurs in mid-June, while NDVI derived from spectral data acquired in September consistently showed lower correlations with species diversity. This highlights a well-recognized characteristic of the SVH: its strong dependence on seasonality (Rossi et al., 2024; Torresani et al., 2018; Rossi et al., 2021a). Vegetation phenology changes throughout the year, influencing canopy reflectance and, consequently, the strength of SH–biodiversity relationships. Therefore, the results presented here can be considered a “snapshot” specific to early autumn conditions. It is likely that if EnMAP imagery had been available for other phenological stages—such as peak greenness in June—different results would have emerged, potentially favoring the VI and improving the overall predictive power of SH metrics. It is worth noting that our approach based on VIs comes with some limitations. First, the selection of specific EnMAP bands used to compute each

VI was guided by existing literature; however, alternative or adjacent bands—particularly in the NIR region—might have yielded slightly different results, and this band selection choice could influence SH estimates. Second, our calculation of the CV relied on the absolute mean to ensure numerical stability in the presence of negative or near-zero VI values, as found in indices such as NDWI or BGI. While this approach prevents inflated CV values due to small denominators, it may also reduce sensitivity to subtle spectral variation across plots. Future studies could explore normalization strategies or alternative formulations to further refine the robustness of SH–diversity relationships based on VIs.

Strongest results were observed when SH was computed across entire spectral ranges, such as the VIS, NIR, and SWIR regions. This approach, which integrates broader spectral information rather than individual bands, was also tested by Wang et al. (2018a), who evaluated the SVH by examining the relationship between spectral variability—expressed as the CV—and Simpson's diversity index in a prairie grassland. They found that at fine spatial scales (e.g., 1 mm to 10 cm), CV calculated from the VIS (430–700 nm) was more strongly correlated with biodiversity than CV from the NIR (700–900 nm). However, as pixel size increased, the relationship between NIR-derived CV and biodiversity became stronger, eventually outperforming the VIS at coarser resolutions (25–50 cm). These findings suggest that the predictive power of different spectral regions may vary with spatial resolution and structural complexity. Although their ecological context differs from ours (prairie vs. forest), our study supports a similar conclusion, SH calculated over the NIR region consistently outperformed VIS and SWIR in predicting tree species diversity. This may reflect the ability of NIR wavelengths to capture, as previously stated, structural and compositional differences in forest canopies, which are critical indicators of biodiversity. Also Gholizadeh et al. (2018b) showed that SH calculated from the NIR region exhibited stronger correlations with plant species richness than from the VIS when the spatial resolution was coarse, likely due to the NIR's sensitivity to vegetation structure. Together, these results reinforce the importance of spectral region selection in biodiversity studies and suggest that NIR, particularly at moderate resolutions such as those offered by EnMAP, is especially relevant for forest biodiversity assessment.

4.2. Evaluating the impact of spatial approaches on SH–diversity relationships

Our results clearly highlight the importance of spatial approach selection when testing the SVH. Among the three tested approaches—(A) the normal (equal weight) method, (B) the weighted-area method, and (C) the weighted-area method considering only plots with CC > 70%—the latter two consistently outperformed the normal approach in terms of R^2 values across all spectral analyses. The normal approach, which assigns equal weight to each of the four EnMAP pixels intersecting a plot, produced the weakest correlations between SH and tree species diversity. This outcome is likely due to the spatial mismatch between pixel boundaries and actual plot extent, where pixels may contribute less-representative spectral information that dilutes the signal relevant to field data. Such mismatches are a well-documented limitation in remote sensing applications when the spatial grain of the imagery does not align with ecological sampling units (Gamon et al., 2020; Moudry et al., 2023).

In contrast, the weighted-area approach—which weights each pixel based on its proportion of spatial overlap with the field plot—demonstrated significantly stronger correlations. This method more accurately reflects the actual spatial contribution of each pixel to the sampled area especially in our case where the difference in size between the pixel spectral reflectance (90 m × 90 m) and plot size (26 m diameter) is relatively high. To our knowledge, this is the first study to implement such an area-based weighting method for SH calculation in the context of the SVH using spaceborne hyperspectral data. This

advancement contributes a novel methodological improvement, aligning SH estimation more closely with ecological field conditions and enhancing the reliability of remote sensing-based biodiversity proxies. We are nonetheless aware of the limitations inherent in this approach. Specifically, uncertainties in plot geolocation and in the geometric correction of EnMAP imagery may introduce spatial misalignments that affect SH calculations. Even small mismatches between field plots and pixel boundaries could propagate into errors in the estimation of SH. However, such spatial uncertainties are a well-recognized and often unavoidable challenge in remote sensing applications, particularly when integrating field data with satellite-derived information (Moudrý et al., 2023). As in many SVH studies, we acknowledge this limitation while striving to minimize its impact through careful data processing and methodological refinement. The best results were obtained using the third approach, which applied the weighted-area method exclusively to plots with a CC greater than 70%. The superior performance can be attributed to the reduction of confounding factors such as soil background reflectance. This methodological refinement aligns with findings by Gholizadeh et al. (2018b), who demonstrated that soil exposure can significantly confound spectral diversity assessments in prairie ecosystems. By focusing on plots with high CC, our approach minimizes the influence of non-vegetative elements, thereby enhancing the accuracy of biodiversity estimations. Similarly Wang et al. (2022b) addressed the influence of vegetation percent cover on the SH-biodiversity relationship correcting for soil effects by using vegetation percent cover (estimated through visual interpretation) to adjust their SH indices. This filtering effect has implications beyond spectral measurements. It also influences the structural-biodiversity relationship described in the Height Variation Hypothesis (HVH), which links vertical canopy complexity to species richness and composition (Torresani et al., 2023b, 2024b). Studies have shown that structural metrics, such as canopy height variation derived from LiDAR, tend to correlate more strongly with species diversity in closed-canopy, where vertical layering is well-developed and less obscured by non-vegetative elements (Hakkenberg et al., 2016, 2023). Conversely, in open areas or plots with sparse vegetation cover, the lack of vertical structure and the increased influence of ground features can weaken this relationship.

This adds a valuable contribution and a methodological reference point for future work. While LiDAR data was essential in our study for identifying high-canopy-cover plots, we agree that the unavailability of ALS data should not be considered a barrier to implementing this framework more broadly. Emerging alternatives may help overcome this limitation. For example, the recently released global CHM at 1 m spatial resolution, developed by Meta and World Resource Institute (Tolan et al., 2024), based on GEDI data (Moudrý et al., 2024c) could serve as a valuable alternative. Preliminary analyses (Torresani et al., 2025) suggest that this dataset can reliably approximate canopy cover in alpine forests. We believe that such resources, especially when available as open-access datasets, offer promising opportunities to replicate and extend our approach in regions lacking high-resolution LiDAR data.

4.3. Influence of field-based diversity metrics and spectral heterogeneity measures

Our results indicate that the correlation between SH and tree species diversity was generally stronger when species richness was used as the field-based diversity metric. This finding is consistent with several studies in the literature (Arekhi et al., 2017) showing that abundance-sensitive metrics, like Shannon's H, can be more affected by mismatches between the spatial scale of field plots and the pixel size of remote sensing imagery (Gamon et al., 2020; Schmidlein and Fassnacht, 2017). In our study, field plots had a diameter of 26 m, while EnMAP pixels are 30×30 m. Although these scales are similar, the pixel footprint still exceeds the plot area, introducing potential signal integration from neighboring vegetation outside the plots. Species richness, which simply counts species presence and is less sensitive to abundance, is

more robust to this type of spatial mismatch. In contrast, Shannon's H relies on accurate species abundance estimates, which may not align well with the spectral signal averaged over a larger pixel area, thereby weakening correlations with SH (Rocchini et al., 2010; Torresani et al., 2024c). Moreover, the alpine forests analyzed in our study are characterized by low tree species richness and sparse canopy gaps, which may amplify the effects of pixel-plot scale discrepancies. Such environments can lead to mixed spectral signals within pixels, especially when plots are near ecotones or contain small openings, further affecting abundance-weighted metrics like Shannon's H. This is in line with findings from Gamon et al. (2020) and Moudrý et al. (2023), who emphasize the importance of scale alignment for reliable optical-diversity relationships. These results highlight the critical need to carefully consider spatial scale when analyzing SH-biodiversity relationships (Torresani et al., 2024c). Matching field plot size with the resolution of remote sensing imagery—or applying methods that account for scale mismatches—can help improve the accuracy of SH-diversity correlations, particularly when using diversity indices sensitive to species abundances. On the other side, in different SVH studies, stronger correlations have been reported when diversity metrics that account for species abundance, such as Shannon's H (Oldeland et al., 2010; Wang et al., 2016, 2018b; Torresani et al., 2019) are used.

These differences across studies highlight the context-dependent nature of the SH-biodiversity relationship and the ongoing debate regarding the most appropriate field metric to use. These seasonal dynamics emphasize again the importance of the temporal dimension in SVH studies, particularly regarding which diversity metric may perform best depending on phenological stage.

Regarding SH measures, both Rao's Q and the CV showed similar and consistent results when correlated with tree species diversity. This trend was observed across the different analytical scales—individual bands, spectral ranges, and VI—and under all three spatial approaches. This convergence suggests that both heterogeneity indices capture similar aspects of spectral variability relevant to biodiversity, despite their conceptual differences. Rao's Q is a distance-based metric that incorporates pairwise dissimilarities in reflectance across pixels and wavelengths (Thouverai et al., 2022; Rocchini et al., 2024), while CV provides a relative measure of variability by standardizing the standard deviation with the mean reflectance (Rossi et al., 2021b). The fact that both measures perform similarly in our study supports the idea that SH, regardless of how it is quantified, holds meaningful ecological information about species diversity—at least in forest ecosystems like those of the Italian Alps. These results are in line with findings from other studies that have compared multiple SH metrics, such as Tagliabue et al. (2020) and Wang et al. (2022a), which also reported relatively small differences in the predictive power of different heterogeneity indices when applied to species diversity estimation. It is worth to highlight that this study represents, to our knowledge, the first application of a weighted Rao's Q formulation for SH, where pixel contributions are scaled by their proportional overlap with the plot. This approach is conceptually analogous to the weighting strategies previously applied to other heterogeneity metrics, such as the CV (e.g., Wang et al. (2016, 2018a)), and our results suggest that the weighted Rao's Q performs consistently with more established indices. Nevertheless, we acknowledge that further theoretical validation and systematic comparison with alternative formulations represent important directions for future research.

4.4. Limitations

Our research has some inherent limitations that should be acknowledged. A primary limitation of our study is the temporal mismatch between field-based tree diversity data (collected between 2021 and 2024) and the EnMAP imagery (acquired in September 2023) (Ferrara et al., 2023). This multi-year sampling period introduces the

possibility that shifts in species composition, tree mortality, recruitment, or forest management activities could have occurred between the field surveys and the satellite acquisition (Ferrara et al., 2023). Such temporal discrepancies can weaken the relationship between SH and field-based diversity measures because they effectively compare observations from different ecological moments. While we believe the stable nature of alpine forest ecosystems minimizes the likelihood of major changes during this period—given slow growth rates and limited anthropogenic disturbance—some variability cannot be excluded, especially for small-scale disturbances (e.g., windthrows, localized pest outbreaks) that might not have been recorded but could impact canopy structure or composition. Moreover, phenological differences across years could further affect comparisons if spectral properties of the canopy (e.g., pigment concentrations) varied with interannual climate fluctuations. Such discrepancies could potentially introduce bias, but they are relatively common in remote sensing studies—and particularly in SVH research (Torresani et al., 2024c)—due to logistical and operational constraints. This challenge is even more pronounced when working with satellite systems like EnMAP, which require on-demand data requests rather than providing continuous, open-access imagery as with platforms like Sentinel-2 or Landsat (Carmona et al., 2024). The need to coordinate limited acquisition windows with field campaigns highlights the critical importance of advancing open-source data policies in Earth observation missions (Rocchini and Neteler, 2012). Broader availability of timely, high-resolution hyperspectral data would facilitate better alignment between field measurements and imagery, ultimately strengthening the accuracy and applicability of studies linking SH to biodiversity.

A similar issue applies to the ALS data used to assess CC, which were collected in 2006—the only LiDAR dataset available for the region. As for the previous limitation, this temporal gap between the ALS data and the EnMAP imagery could, in principle, introduce uncertainty due to possible changes in forest structure over time. Such changes might stem from natural disturbances, management interventions, or successional dynamics leading to gradual shifts in canopy closure and vertical structure (Seidl et al., 2014). While we consider this impact minimal in our case, it should be regarded as a potential source of bias in interpreting absolute CC values and in extending these findings to other forest types or regions with faster structural dynamics. In ecological studies, however, temporal mismatches between ALS and field data are relatively common and have been shown not to necessarily compromise the validity of results. For example, McRoberts et al. (2018) demonstrated that ALS data can retain utility for forest inventory purposes even when collected more than 10 years before field measurements, reporting reliable estimators with a 12-year lag. Similarly, Hill and Hinsley (2015) showed that ALS data could still yield meaningful organism–habitat relationships despite field data being collected up to 15 years after the LiDAR acquisition. Several lines of evidence suggest furthermore that the practical impact of this temporal offset is limited in our case. First, we have direct and repeated knowledge of the plots, which we have monitored and remeasured in multiple field campaigns. These repeated observations did not reveal substantial changes in tree density, species composition, or canopy closure across the plots. Second, the study area is dominated by montane and alpine forests characterized by slow growth rates and minimal anthropogenic disturbance. The harsh climatic conditions of these high-altitude environments—marked by short growing seasons, prolonged snow cover, and limited productivity—naturally constrain rapid structural changes. Third, none of the plots included in the analysis were affected by known recent disturbances documented in local forest monitoring programs. As such, although the age of the ALS data represents an unavoidable limitation due to the lack of updated LiDAR acquisitions, we believe it has minimal influence on our key findings. Nonetheless, it is important to recognize that this type of limitation is common in studies relying on ALS data, which are not always easily accessible and often involve a temporal mismatch with more recent remote sensing imagery (Asner et al., 2012; Coomes et al.,

2017). This situation highlights the critical need also for more frequent, updated, and openly available ALS datasets, especially given that the costs of conducting LiDAR flights have been decreasing in recent years (Moudry et al., 2021). Ensuring broader access to up-to-date ALS data would greatly improve the accuracy of canopy structure estimates and strengthen studies that integrate structural information with SH for biodiversity monitoring.

Another potential limitation relates to the relatively low tree species richness in our alpine forest plots. This is substantially lower than in, e.g., tropical forests, where diversity can exceed several hundred species per hectare. However, such low diversity is typical of alpine environments, shaped, as previously stated, by harsh climatic conditions and nutrient-poor soils—which naturally constrain species richness and composition. Importantly, previous remote sensing studies have shown that meaningful SH–diversity relationships can still be detected in species-poor ecosystems. For instance, Torresani et al. (2019) reported SH–diversity links in alpine conifer forests where plot-level richness reached up to 7 species and Shannon's diversity ranged from 0.1 to 1.4, while Wang et al. (2022a) demonstrated similar patterns in mangrove stands with 1–5 species and Shannon's index between 0 and 1.55. These richness and diversity ranges are comparable to those in our study (1–4 species; Shannon's index 0.14–1.36). In ecosystems with higher species richness and more complex assemblages, the relationships between SH and biodiversity may differ substantially due to increased spectral overlap among co-occurring species, higher canopy layering, or diverse structural traits (Gamon et al., 2020). As a result, the strength of SH–biodiversity relationships observed here cannot be assumed to generalize directly to ecosystems with greater floristic complexity. Moreover, while lower species richness can simplify interpretation by reducing spectral confounding at moderate spatial resolutions (e.g., 30 m), it may also limit the ecological insight gained from SH metrics by failing to capture the spectral complexity present in more diverse forests. Therefore, although our study provides valuable initial evidence of the potential for EnMAP-based SH to estimate diversity in alpine forests, future research should extend these analyses to ecosystems with broader species richness gradients to more fully evaluate the robustness and transferability of the SVH across different biodiversity contexts. Possible approaches include the use of radiative transfer simulations (e.g., PROSAIL or forest-specific canopy models) to generate synthetic reflectance scenarios with higher diversity levels, as well as cross-site comparisons with datasets from temperate or tropical forests where tree diversity is substantially greater. These strategies would provide valuable benchmarks for evaluating whether the relationships detected in species-poor alpine systems hold under more species-rich conditions.

Lastly, the number of usable plots could be viewed as a limitation. Of the 52 field plots initially available, only 42 were ultimately used due to corrupted or incomplete spectral data in certain areas. While a larger sample size would increase statistical power, it is worth noting that other SVH studies have successfully demonstrated meaningful relationships using comparable or even fewer plots. For instance, Wang et al. (2018a) conducted detailed SVH analyses using a limited number of plots in prairie ecosystems. Gould (2000) assessed SH in just 17 forest plots in the Hood River region of the Central Canadian Arctic. Xu et al. (2022) tested SVH relationships using 18 sample plots in alpine steppe at the Sanjiangyuan National Nature Reserve, Qinghai Province, China. Similarly, Végh and Tsuyuzaki (2021) investigated the effects of image resolution on SH–biodiversity relationships within 35 forest plots in Mount Usu, located in the temperate region of northern Japan. Given that this study represents one of the first applications of EnMAP data in alpine forests, the inclusion of 42 high-quality, well-characterized plots is still a strong foundation for preliminary assessment.

Taken together, while these limitations highlight areas for future improvement, they do not detract from the overall validity of our findings. Rather, they underscore the need for continued research across diverse ecosystems, temporal scales, and data availability conditions.

5. Conclusions

This study tested the SVH using EnMAP hyperspectral data to assess tree species diversity in forest ecosystems, demonstrating that the correlation between SH and species diversity can be effective under certain conditions. Our findings highlight the potential of EnMAP data for biodiversity monitoring, complementing traditional field-based assessments, particularly when SH is calculated in specific spectral regions. However, several limitations and knowledge gaps remain. Notably, this study was based on a single EnMAP image acquired in early autumn, and we were therefore unable to assess seasonal variation in the SH–biodiversity relationship. The temporal dimension remains a critical aspect of SVH research, especially in forest ecosystems where phenological changes can influence both spectral signals and species detectability. To date, multi-temporal analyses using spaceborne hyperspectral data remain largely unexplored, and future studies should prioritize this direction to better understand the seasonal dynamics of biodiversity patterns. In addition, further research is needed to address remaining uncertainties in the SVH framework. For example, exploring the relationship between SH and diversity across different taxa—such as understory vegetation, fungi, or fauna—would offer valuable insights into the broader ecological applications of hyperspectral remote sensing. Future studies could also focus on integrating sub-pixel spectral unmixing techniques (Rossi and Gholizadeh, 2023) to reduce the influence of mixed pixels and enhance the reliability of SH estimates, especially when working with moderate-resolution sensors like EnMAP. Additionally, assessing beta diversity using hyperspectral data represents a promising direction for future research as done in recent studies (Bongalov et al., 2019) in order to capture spatial patterns of biodiversity beyond local (alpha) diversity. Finally, integrating SVH with structural information derived from LiDAR or radar data, as shown in previous studies (Torresani et al., 2020; Tamburlin et al., 2021), may enhance biodiversity estimation, especially in forests where vertical structure and canopy complexity are key drivers of diversity (Hakkenberg et al., 2016, 2023). Such integrative approaches hold great promise for advancing remote sensing-based biodiversity monitoring, enabling more robust, temporally explicit, and ecologically meaningful assessments across spatial and biological scales.

CRediT authorship contribution statement

Michele Torresani: Writing – original draft, Visualization, Validation, Methodology, Investigation, Formal analysis, Conceptualization. **Christian Rossi:** Writing – review & editing, Visualization, Methodology, Investigation, Conceptualization. **Marco Mina:** Writing – review & editing, Methodology, Investigation. **Irene Menegaldo:** Writing – review & editing, Methodology. **Matteo Cappuccio:** Methodology. **Michela Perrone:** Writing – review & editing, Methodology, Investigation, Conceptualization. **Christopher R. Hakkenberg:** Writing – review & editing, Methodology, Investigation, Conceptualization. **Duccio Rocchini:** Writing – review & editing, Methodology, Investigation, Conceptualization. **Nicola Puletti:** Writing – review & editing, Methodology. **Laura Stendardi:** Writing – review & editing, Methodology. **Leonardo Montagnani:** Writing – review & editing, Methodology. **Roberto Tognetti:** Writing – review & editing, Validation, Supervision, Methodology, Conceptualization.

Declaration of Generative AI and AI-assisted technologies in the writing process

During the preparation of this work, the authors utilized AI software (ChatGPT) to enhance the phrasing, spelling, and grammar of the manuscript. After employing this tool, the authors reviewed and edited the content as necessary and assume full responsibility for the content of the publication.

Funding

MT, CR, MM and RT are partially funded by the “MAP-Rezia” (ID 0200061) project within the Interreg VI-A Italy–Switzerland Program.

Declaration of competing interest

The authors declare the following financial interests/personal relationships which may be considered as potential competing interests: Michele Torresani reports financial support was provided by Interreg Italy–Switzerland MAP-Rezia project. If there are other authors, they declare that they have no known competing financial interests or personal relationships that could have appeared to influence the work reported in this paper.

Acknowledgments

The authors thank the Department of Innovation, Research, University and Museums of the Autonomous Province of Bozen/Bolzano for covering the Open Access publication costs.

Appendix A. Supplementary data

Supplementary material related to this article can be found online at <https://doi.org/10.1016/j.jag.2025.104902>.

Data availability

All data supporting the findings of this study are included within the manuscript and its supplementary materials. The satellite data (EnMAP Level-2A products) used in the analysis are publicly available through the EnMAP Instrument Planning Portal. The scripts used are available upon reasonable request.

References

- Affinito, F., Williams, J.M., Campbell, J.E., Londono, M.C., Gonzalez, A., 2024. Progress in developing and operationalizing the monitoring framework of the global biodiversity framework. *Nat. Ecol. Evol.* 8 (12), 2163–2171.
- Arekhi, M., Yilmaz, O.Y., Yilmaz, H., Akyuz, Y.F., 2017. Can tree species diversity be assessed with landsat data in a temperate forest? *Environ. Monit. Assess.* 189, 1–14.
- Asner, G.P., Clark, J.K., Mascaro, J., Galindo García, G., Chadwick, K.D., Navarrete Encinales, D., Paez-Acosta, G., Cabrera Montenegro, E., Kennedy-Bowdoin, T., Duque, Á., et al., 2012. High-resolution mapping of forest carbon stocks in the Colombian Amazon. *Biogeosciences* 9 (7), 2683–2696.
- Bae, S., Levick, S.R., Heidrich, L., Magdon, P., Leutner, B.F., Wöllauer, S., Seribryanyk, A., Nauss, T., Krzystek, P., Gossner, M.M., et al., 2019. Radar vision in the mapping of forest biodiversity from space. *Nat. Commun.* 10 (1), 4757.
- Bongalov, B., Burslem, D.F., Jucker, T., Thompson, S.E., Rosindell, J., Swinfield, T., Nilus, R., Clewley, D., Phillips, O.L., Coomes, D.A., 2019. Reconciling the contribution of environmental and stochastic structuring of tropical forest diversity through the lens of imaging spectroscopy. *Ecol. Lett.* 22 (10), 1608–1619.
- Botta-Dukát, Z., 2005. Rao's quadratic entropy as a measure of functional diversity based on multiple traits. *J. Veg. Sci.* 16 (5), 533–540.
- Brokerhoff, E.G., Barbaro, L., Castagneyrol, B., Forrester, D.I., Gardiner, B., González-Olabarria, J.R., Lyver, P.O., Meurisse, N., Oxbrough, A., Taki, H., et al., 2017. Forest biodiversity, ecosystem functioning and the provision of ecosystem services.
- Carmona, E., Chabriat, S., Fischer, S., Habermeyer, M., La Porta, L., Mühlé, H., Pinnel, N., Pato, M., Wirth, K., 2024. ENMAP operations status. In: IGARSS 2024–2024 IEEE International Geoscience and Remote Sensing Symposium. IEEE, pp. 292–295.
- Cavender-Bares, J., Schneider, F.D., Santos, M.J., Armstrong, A., Carnaval, A., Dahlin, K.M., Fatoyinbo, L., Hurt, G.C., Schimel, D., Townsend, P.A., et al., 2022. Integrating remote sensing with ecology and evolution to advance biodiversity conservation. *Nat. Ecol. Evol.* 6 (5), 506–519.
- Cazzolla Gatti, R., Reich, P.B., Gamarrá, J.G., Crowther, T., Hui, C., Morera, A., Bastin, J.-F., De-Miguel, S., Nabuurs, G.-J., Svenning, J.-C., et al., 2022. The number of tree species on earth. *Proc. Natl. Acad. Sci.* 119 (6), e2115329119.
- Chabriat, S., Foerster, S., Segl, K., Beamish, A., Brell, M., Asadzadeh, S., Milewski, R., Ward, K.J., Brosinsky, A., Koch, K., et al., 2024. The EnMAP spaceborne imaging spectroscopy mission: Initial scientific results two years after launch. *Remote Sens. Environ.* 315, 114379.

- Conti, L., Malavasi, M., Galland, T., Komárek, J., Lagner, O., Carmona, C.P., De Bello, F., Rocchini, D., Šimová, P., 2021. The relationship between species and spectral diversity in grassland communities is mediated by their vertical complexity. *Appl. Veg. Sci.* 24 (3).
- Coomes, D.A., Dalponte, M., Jucker, T., Asner, G.P., Banin, L.F., Burslem, D.F., Lewis, S.L., Nilus, R., Phillips, O.L., Phua, M.-H., et al., 2017. Area-based vs tree-centric approaches to mapping forest carbon in Southeast Asian forests from airborne laser scanning data. *Remote Sens. Environ.* 194, 77–88.
- EnMAP Ground Segment Team, 2023. Level 2A processor (atmospheric correction over land) – algorithm theoretical baseline document. https://www.enmap.org/data/doc/EN-PCV-TN-6007_Level_2A_Processor_Atmospheric_Correction_Land.pdf.
- EnMAP Ground Segment, Doc. ID EN-PCV-TN-6007, Issue 2.4, 07 September 2023.
- ESA eoPortal, 2025. Enmap (environmental mapping and analysis program). Accessed: 2025-01-16.
- Esquivel, J., Echeverría, C., Saldaña, A., Fuentes, R., 2020. High functional diversity of forest ecosystems is linked to high provision of water flow regulation ecosystem service. *Ecol. Indic.* 115, 106433.
- Fassnacht, F.E., Müllerová, J., Conti, L., Malavasi, M., Schmidlein, S., 2022. About the link between biodiversity and spectral variation. *Appl. Veg. Sci.* 25 (1), e12643.
- Ferrara, C., Chianucci, F., Bajocco, S., 2023. On the temporal mismatch between in-situ and satellite-derived spring phenology of European beech forests. *Int. J. Remote Sens.* 44 (5), 1684–1701.
- Foody, G., 2008. GIS: biodiversity applications. *Prog. Phys. Geogr.* 32 (2), 223–235.
- Gamon, J.A., Wang, R., Gholizadeh, H., Zutta, B., Townsend, P.A., Cavender-Bares, J., 2020. Consideration of scale in remote sensing of biodiversity. *Remote. Sens. Plant Biodivers.* 425–447.
- Gatti, R.C., Lobos, R.B.C., Torresani, M., Rocchini, D., 2025. An early warning system based on machine learning detects huge forest loss in Ukraine during the war. *Glob. Ecol. Conserv.* 58, e03427.
- Gholizadeh, H., Dixon, A.P., Pan, K.H., McMillan, N.A., Hamilton, R.G., Fuhldorf, S.D., Cavender-Bares, J., Gamon, J.A., 2022. Using airborne and DESIS imaging spectroscopy to map plant diversity across the largest contiguous tract of tallgrass prairie on earth. *Remote Sens. Environ.* 281, 113254.
- Gholizadeh, H., Gamon, J.A., Townsend, P.A., Zygielbaum, A.I., Helzer, C.J., Hmimina, G.Y., Yu, R., Moore, R.M., Schweiger, A.K., Cavender-Bares, J., 2019. Detecting prairie biodiversity with airborne remote sensing. *Remote Sens. Environ.* 221, 38–49.
- Gholizadeh, H., Gamon, J.A., Zygielbaum, A.I., Wang, R., Schweiger, A.K., Cavender-Bares, J., 2018b. Remote sensing of biodiversity: Soil correction and data dimension reduction methods improve assessment of α -diversity (species richness) in prairie ecosystems. *Remote Sens. Environ.* 206, 240–253.
- Gholizadeh, H., Žižala, D., Saberioon, M., Borůvka, L., 2018a. Soil organic carbon and texture retrieving and mapping using proximal, airborne and sentinel-2 spectral imaging. *Remote Sens. Environ.* 218, 89–103.
- Gillespie, T.W., 2005. Predicting woody-plant species richness in tropical dry forests: a case study from South Florida, USA. *Ecol. Appl.* 15 (1), 27–37.
- Gould, W., 2000. Remote sensing of vegetation, plant species richness, and regional biodiversity hotspots. *Ecol. Appl.* 10 (6), 1861–1870.
- Hakkenberg, C., Atkins, J., Brodie, J., Burns, P., Cushman, S., Jantz, P., Kasztza, Z., Quinn, C., Rose, M., Goetz, S., 2023. Inferring alpha, beta, and gamma plant diversity across biomes with GEDI spaceborne lidar. *Environ. Res.: Ecol.* 2 (3), 035005.
- Hakkenberg, C.R., Song, C., Peet, R.K., White, P.S., 2016. Forest structure as a predictor of tree species diversity in the North Carolina Piedmont. *J. Veg. Sci.* 27 (6), 1151–1163.
- Hakkenberg, C., Zhu, K., Peet, R., Song, C., 2018. Mapping multi-scale vascular plant richness in a forest landscape with integrated LiDAR and hyperspectral remote-sensing. *Ecology* 99 (2), 474–487.
- Hall, K., Johansson, L.J., Sykes, M., Reitalu, T., Larsson, K., Prentice, H.C., 2010. Inventory management status and plant species richness in semi-natural grasslands using high spatial resolution imagery. *Appl. Veg. Sci.* 13 (2), 221–233.
- Hauser, L.T., Timmermans, J., van der Windt, N., Sil, Á.F., de Sá, N.C., Soudzilovskaja, N.A., van Bodegom, P.M., 2021. Explaining discrepancies between spectral and in-situ plant diversity in multispectral satellite earth observation. *Remote Sens. Environ.* 265, 112684.
- Helfenstein, I.S., Schneider, F.D., Schaepman, M.E., Morsdorf, F., 2022. Assessing biodiversity from space: Impact of spatial and spectral resolution on trait-based functional diversity. *Remote Sens. Environ.* 275, 113024.
- Hill, R.A., Hinsley, S.A., 2015. Airborne lidar for woodland habitat quality monitoring: Exploring the significance of lidar data characteristics when modelling organism-habitat relationships. *Remote. Sens.* 7 (4), 3446–3466.
- Jung, M., 2022. Predictability and transferability of local biodiversity environment relationships. *PeerJ* 10, e13872.
- Kaufmann, H., Segl, K., Chabirillat, S., Hofer, S., Stuffer, T., Mueller, A., Richter, R., Schreier, G., Haydn, R., Bach, H., 2006. EnMAP a hyperspectral sensor for environmental mapping and analysis. In: 2006 IEEE International Symposium on Geoscience and Remote Sensing. IEEE, pp. 1617–1619.
- Knyazikhin, Y., Schull, M.A., Stenberg, P., Möttus, M., Rautiainen, M., Yang, Y., Marshak, A., Latorre Carmona, P., Kaufmann, R.K., Lewis, P., et al., 2013. Hyperspectral remote sensing of foliar nitrogen content. *Proc. Natl. Acad. Sci.* 110 (3), E185–E192.
- Levin, N., Shmida, A., Levanon, O., Tamari, H., Kark, S., 2007. Predicting mountain plant richness and rarity from space using satellite-derived vegetation indices. *Diversity and Distributions* 13 (6), 692–703.
- Lopes, M., Fauvel, M., Ouin, A., Girard, S., 2017. Spectro-temporal heterogeneity measures from dense high spatial resolution satellite image time series: Application to grassland species diversity estimation. *Remote. Sens.* 9 (10), 993.
- Mapfumo, R.B., Murwira, A., Masocha, M., Andriani, R., 2016. The relationship between satellite-derived indices and species diversity across African savanna ecosystems. *Int. J. Appl. Earth Obs. Geoinf.* 52, 306–317.
- McRoberts, R.E., Chen, Q., Gormanson, D.D., Walters, B.F., 2018. The shelf-life of airborne laser scanning data for enhancing forest inventory inferences. *Remote. Sens. Environ.* 206, 254–259.
- Moudrý, V., Bazzichetto, M., Remelgado, R., Devillers, R., Lenoir, J., Mateo, R.G., Lembrechts, J.J., Sillero, N., Lecours, V., Cord, A.F., et al., 2024a. Optimising occurrence data in species distribution models: sample size, positional uncertainty, and sampling bias matter. *Ecography* 2024 (12), e07294.
- Moudrý, V., Gábor, L., Marselis, S., Pracná, P., Barták, V., Prošek, J., Navratilova, B., Novotný, J., Potůčková, M., Gdulová, K., et al., 2024b. Comparison of three global canopy height maps and their applicability to biodiversity modeling: Accuracy issues revealed. *Ecosphere* 15 (10), e70026.
- Moudrý, V., Keil, P., Gábor, L., Lecours, V., Zarzo-Arias, A., Barták, V., Malavasi, M., Rocchini, D., Torresani, M., Gdulová, K., et al., 2023. Scale mismatches between predictor and response variables in species distribution modelling: A review of practices for appropriate grain selection. *Prog. Phys. Geogr.: Earth Environ.* 47 (3), 467–482.
- Moudrý, V., Moudrá, L., Barták, V., Bejček, V., Gdulová, K., Hendrychová, M., Moravec, D., Musil, P., Rocchini, D., Šťastný, K., et al., 2021. The role of the vegetation structure, primary productivity and senescence derived from airborne LiDAR and hyperspectral data for birds diversity and rarity on a restored site. *Landscape Urban Plan.* 210, 104064.
- Moudrý, V., Prošek, J., Marselis, S., Marešová, J., Šárovcová, E., Gdulová, K., Kozhoridze, G., Torresani, M., Rocchini, D., Eltner, A., et al., 2024c. How to find accurate terrain and canopy height GEDI footprints in temperate forests and grasslands? *Earth Space Sci.* 11 (10), e2024EA003709.
- Moura, M.R., Jetz, W., 2021. Shortfalls and opportunities in terrestrial vertebrate species discovery. *Nat. Ecol. Evol.* 5 (5), 631–639.
- Nagendra, H., 2001. Using remote sensing to assess biodiversity. *Int. J. Remote Sens.* 22 (12), 2377–2400.
- Oindo, B.O., Skidmore, A.K., 2002. Interannual variability of NDVI and species richness in Kenya. *Int. J. Remote Sens.* 23 (2), 285–298.
- Oldeland, J., Weslus, D., Rocchini, D., Schmidt, M., Jürgens, N., 2010. Does using species abundance data improve estimates of species diversity from remotely sensed spectral heterogeneity? *Ecol. Indic.* 10 (2), 390–396.
- Onishi, M., Ise, T., 2021. Explainable identification and mapping of trees using UAV RGB image and deep learning. *Sci. Rep.* 11 (1), 903.
- Pacheco-Labrador, J., Migliavacca, M., Ma, X., Mahecha, M., Carvalhais, N., Weber, U., Benavides, R., Bouriaud, O., Barnoaeia, I., Coomes, D.A., et al., 2022. Challenging the link between functional and spectral diversity with radiative transfer modeling and data. *Remote Sens. Environ.* 280, 113170.
- Pafumi, E., Petruzzellis, F., Castello, M., Altobelli, A., Maccherini, S., Rocchini, D., Bacaro, G., 2023. Using spectral diversity and heterogeneity measures to map habitat mosaics: An example from the classical Karst. *Appl. Veg. Sci.* 26 (4), e12762.
- Palmer, M.W., Earls, P.G., Hoagland, B.W., White, P.S., Wohlgemuth, T., 2002. Quantitative tools for perfecting species lists. *Environ.: Off. J. Int. Environ. Soc.* 13 (2), 121–137.
- Perrone, M., Conti, L., Galland, T., Komárek, J., Lagner, O., Torresani, M., Rossi, C., Carmona, C.P., de Bello, F., Rocchini, D., et al., 2024. “Flower power”: How flowering affects spectral diversity metrics and their relationship with plant diversity. *Ecol. Inf.* 81, 102589.
- Perrone, M., Di Febraro, M., Conti, L., Divišek, J., Chytrý, M., Keil, P., Carranza, M.L., Rocchini, D., Torresani, M., Moudrý, V., et al., 2023. The relationship between spectral and plant diversity: Disentangling the influence of metrics and habitat types at the landscape scale. *Remote. Sens. Environ.* 293, 113591.
- Pinon, T.B.M., Mendonça, A.R.D., Silva, G.F.D., Effgen, E.M., Rodrigues, N.M.M., Fernandes, M.M., Sansevero, J.B.B., Almeida, C.T.D., Dias, H.M., Gonçalves, F.G., et al., 2024. Biodiversity from the sky: Testing the spectral variation hypothesis in the Brazilian Atlantic forest. *Remote. Sens.* 16 (23), 4363.
- Rahmanian, S., Nasiri, V., Amindin, A., Karami, S., Maleki, S., Pouyan, S., Borz, S.A., 2023. Prediction of plant diversity using multi-seasonal remotely sensed and geodiversity data in a mountainous area. *Remote. Sens.* 15 (2), 387.
- Rao, C.R., 1982. Diversity and dissimilarity coefficients: a unified approach. *Theor. Popul. Biol.* 21 (1), 24–43.
- Reddy, C.S., 2021. Remote sensing of biodiversity: what to measure and monitor from space to species? *Biodivers. Conserv.* 30 (10), 2617–2631.
- Rocchini, D., Balkenhol, N., Carter, G.A., Foody, G.M., Gillespie, T.W., He, K.S., Kark, S., Levin, N., Lucas, K., Luoto, M., et al., 2010. Remotely sensed spectral heterogeneity as a proxy of species diversity: recent advances and open challenges. *Ecol. Inf.* 5 (5), 318–329.

- Rocchini, D., Chiarucci, A., Loiselle, S.A., 2004. Testing the spectral variation hypothesis by using satellite multispectral images. *Acta Oecologica* 26 (2), 117–120.
- Rocchini, D., Dadalt, L., Delucchi, L., Neteler, M., Palmer, M., 2014. Disentangling the role of remotely sensed spectral heterogeneity as a proxy for North American plant species richness. *Community Ecol.* 15 (1), 37–43.
- Rocchini, D., Neteler, M., 2012. Let the four freedoms paradigm apply to ecology. *Trends Ecol. Evolut.* 27 (6), 310–311.
- Rocchini, D., Torresani, M., Beierkuhnlein, C., Feoli, E., Foody, G.M., Lenoir, J., Malavasi, M., Moudrý, V., Šimová, P., Ricotta, C., 2022. Double down on remote sensing for biodiversity estimation: a biological mindset. *Community Ecol.* 23 (3), 267–276.
- Rocchini, D., Torresani, M., Ricotta, C., 2024. On the mathematical properties of spatial Rao's Q to compute ecosystem heterogeneity. *Theor. Ecol.* 17 (3), 247–254.
- Rossi, C., Gholizadeh, H., 2023. Uncovering the hidden: Leveraging sub-pixel spectral diversity to estimate plant diversity from space. *Remote Sens. Environ.* 296, 113734.
- Rossi, C., Kneubühler, M., Schütz, M., Schaeppman, M.E., Haller, R.M., Risch, A.C., 2021a. Remote sensing of spectral diversity: A new methodological approach to account for spatio-temporal dissimilarities between plant communities. *Ecol. Indic.* 130, 108106.
- Rossi, C., Kneubühler, M., Schütz, M., Schaeppman, M.E., Haller, R.M., Risch, A.C., 2021b. Spatial resolution, spectral metrics and biomass are key aspects in estimating plant species richness from spectral diversity in species-rich grasslands. *Remote. Sens. Ecol. Conserv.*
- Rossi, C., McMillan, N.A., Schweizer, J.M., Gholizadeh, H., Groen, M., Ioannidis, N., Hauser, L.T., 2024. Parcel level temporal variance of remotely sensed spectral reflectance predicts plant diversity. *Environ. Res. Lett.*
- van der Sande, M.T., Poorter, L., Kooistra, L., Balvanera, P., Thonicke, K., Thompson, J., Arends, E.J., García Alaniz, N., Jones, L., Mora, F., et al., 2017. Biodiversity in species, traits, and structure determines carbon stocks and uptake in tropical forests. *Biotropica* 49 (5), 593–603.
- Schmidlein, S., Fassnacht, F.E., 2017. The spectral variability hypothesis does not hold across landscapes. *Remote Sens. Environ.* 192, 114–125.
- Schneider, F.D., Morsdorf, F., Schmid, B., Petzsch, O.L., Hueni, A., Schimel, D.S., Schaeppman, M.E., 2017. Mapping functional diversity from remotely sensed morphological and physiological forest traits. *Nat. Commun.* 8 (1), 1441.
- Schweiger, A.K., Laliberté, E., 2022. Plant beta-diversity across biomes captured by imaging spectroscopy. *Nat. Commun.* 13 (1), 2767.
- Seidl, R., Schelhaas, M.-J., Rammer, W., Verkerk, P.J., 2014. Increasing forest disturbances in Europe and their impact on carbon storage. *Nat. Clim. Chang.* 4 (9), 806–810.
- Shannon, C.E., 1948. A mathematical theory of communication. *Bell Syst. Tech. J.* 27 (3), 379–423.
- Slaton, M.R., Raymond Hunt, Jr., E., Smith, W.K., 2001. Estimating near-infrared leaf reflectance from leaf structural characteristics. *Am. J. Bot.* 88 (2), 278–284.
- Stein, A., Gerstner, K., Kreft, H., 2014. Environmental heterogeneity as a universal driver of species richness across taxa, biomes and spatial scales. *Ecol. Lett.* 17 (7), 866–880.
- Tagliabue, G., Panigada, C., Celesti, M., Cogliati, S., Colombo, R., Migliavacca, M., Rascher, U., Rocchini, D., Schüttmeyer, D., Rossini, M., 2020. Sun-induced fluorescence heterogeneity as a measure of functional diversity. *Remote Sens. Environ.* 247, 111934.
- Tamburlin, D., Torresani, M., Tomelleri, E., Tonon, G., Rocchini, D., 2021. Testing the height variation hypothesis with the R *rasterdiv* package for tree species diversity estimation. *Remote. Sens.* 13 (18), 3569.
- Thouverai, E., Marcantonio, M., Bacaro, G., Da Re, D., Iannacito, M., Marchetto, E., Ricotta, C., Tattoni, C., Vicario, S., Rocchini, D., 2021. Measuring diversity from space: a global view of the free and open source *rasterdiv* R package under a coding perspective. *Community Ecol.* 1–11.
- Thouverai, E., Marcantonio, M., Lenoir, J., Galfré, M., Marchetto, E., Bacaro, G., Gatti, R.C., Da Re, D., Di Musciano, M., Furrer, R., et al., 2022. Integrals of life: Tracking ecosystem spatial heterogeneity from space through the area under the curve of the parametric Rao's Q index. *Ecol. Complex.* 52, 101029.
- Tolan, J., Yang, H.-I., Nosarzewski, B., Couairon, G., Vo, H.V., Brandt, J., Spore, J., Majumdar, S., Haziza, D., Vamaraju, J., et al., 2024. Very high resolution canopy height maps from RGB imagery using self-supervised vision transformer and convolutional decoder trained on aerial lidar. *Remote Sens. Environ.* 300, 113888.
- Torresani, M., Duccio, R., Marc, Z., Ruth, S., Giustino, T., 2018. Testing the spectral variation hypothesis by using the Rao-Q index to estimate forest biodiversity: Effect of spatial resolution. In: IGARSS 2018-2018 IEEE International Geoscience and Remote Sensing Symposium. IEEE, pp. 1183–1186.
- Torresani, M., Kleijn, D., de Vries, J.P.R., Bartholomeus, H., Chieffallo, L., Gatti, R.C., Moudrý, V., Da Re, D., Tomelleri, E., Rocchini, D., 2023a. A novel approach for surveying flowers as a proxy for bee pollinators using drone images. *Ecol. Indic.* 149, 110123.
- Torresani, M., Montagnani, L., Rocchini, D., Moudrý, V., Andreoli, A., Wellstein, C., Koyanagi, K., Da Ros, L., Bacaro, G., Perrone, M., et al., 2024a. LiDAR insights on stand structure and topography in mountain forest wind extreme events: The Vaia case study. *Agricult. Forest. Meterol.* 359, 110267.
- Torresani, M., Moudrý, V., Hakkenberg, C.R., Barták, V., Rocchini, D., Puliti, S., Hawryl o, P., Sterefíczak, K., Kacic, P., Tognetti, R., 2025. Evaluating the reliability of the 1-meter resolution meta-estimated global canopy height map for estimating forest structural metrics in alpine environment. Manuscript under review in *Forest Ecosystems*.
- Torresani, M., Rocchini, D., Alberti, A., Moudrý, V., Heym, M., Thouverai, E., Kacic, P., Tomelleri, E., 2023b. LiDAR GEDI derived tree canopy height heterogeneity reveals patterns of biodiversity in forest ecosystems. *Ecol. Inf.* 76, 102082.
- Torresani, M., Rocchini, D., Ceola, G., de Vries, J.P.R., Feilhauer, H., Moudrý, V., Bartholomeus, H., Perrone, M., Anderle, M., Gamper, H.A., et al., 2024b. Grassland vertical height heterogeneity predicts flower and bee diversity: an UAV photogrammetric approach. *Sci. Rep.* 14 (1), 809.
- Torresani, M., Rocchini, D., Sonnenschein, R., Zebisch, M., Hauffe, H.C., Heym, M., Pretzsch, H., Tonon, G., 2020. Height variation hypothesis: A new approach for estimating forest species diversity with CHM LiDAR data. *Ecol. Indic.* 117, 106520.
- Torresani, M., Rocchini, D., Sonnenschein, R., Zebisch, M., Marcantonio, M., Ricotta, C., Tonon, G., 2019. Estimating tree species diversity from space in an alpine conifer forest: The Rao's Q diversity index meets the spectral variation hypothesis. *Ecol. Inf.* 52, 26–34.
- Torresani, M., Rossi, C., Perrone, M., Hauser, L.T., Féret, J.-B., Moudrý, V., Simova, P., Ricotta, C., Foody, G.M., Kacic, P., et al., 2024c. Reviewing the spectral variation hypothesis: Twenty years in the tumultuous sea of biodiversity estimation by remote sensing. *Ecol. Inf.* 102702.
- Turner, W., Spector, S., Gardiner, N., Fladeland, M., Sterling, E., Steininger, M., 2003. Remote sensing for biodiversity science and conservation. *Trends Ecol. Evolut.* 18 (6), 306–314.
- Van Cleemput, E., Adler, P., Suding, K.N., 2023. Making remote sense of biodiversity: What grassland characteristics make spectral diversity a good proxy for taxonomic diversity? *Glob. Ecol. Biogeogr.* 32 (12), 2177–2188.
- Végh, L., Tsuyuzaki, S., 2021. Remote sensing of forest diversities: the effect of image resolution and spectral plot extent. *Int. J. Remote Sens.* 42 (15), 5985–6002.
- Wang, R., Gamon, J.A., Cavender-Bares, J., 2022b. Seasonal patterns of spectral diversity at leaf and canopy scales in the Cedar Creek prairie biodiversity experiment. *Remote Sens. Environ.* 280, 113169.
- Wang, R., Gamon, J.A., Cavender-Bares, J., Townsend, P.A., Zygielbaum, A.I., 2018a. The spatial sensitivity of the spectral diversity-biodiversity relationship: an experimental test in a prairie grassland. *Ecol. Appl.* 28 (2), 541–556.
- Wang, R., Gamon, J.A., Emmerton, C.A., Li, H., Nestola, E., Pastorello, G.Z., Menzer, O., 2016. Integrated analysis of productivity and biodiversity in a southern Alberta prairie. *Remote. Sens.* 8 (3), 214.
- Wang, R., Gamon, J.A., Schweiger, A.K., Cavender-Bares, J., Townsend, P.A., Zygielbaum, A.I., Kothari, S., 2018b. Influence of species richness, evenness, and composition on optical diversity: A simulation study. *Remote Sens. Environ.* 211, 218–228.
- Wang, D., Qiu, P., Wan, B., Cao, Z., Zhang, Q., 2022a. Mapping α -and β -diversity of mangrove forests with multispectral and hyperspectral images. *Remote Sens. Environ.* 275, 113021.
- White, J.C., Gómez, C., Wulder, M.A., Coops, N.C., 2010. Characterizing temperate forest structural and spectral diversity with hyperion EO-1 data. *Remote Sens. Environ.* 114 (7), 1576–1589.
- Xu, C., Zeng, Y., Zheng, Z., Zhao, D., Liu, W., Ma, Z., Wu, B., 2022. Assessing the impact of soil on species diversity estimation based on UAV imaging spectroscopy in a natural alpine steppe. *Remote. Sens.* 14 (3), 671.
- Zhao, Y., Sun, Y., Chen, W., Zhao, Y., Liu, X., Bai, Y., 2021. The potential of mapping grassland plant diversity with the links among spectral diversity, functional trait diversity, and species diversity. *Remote. Sens.* 13 (15), 3034.